Inorg. Chem. **2004**, *43*, 101–115

Polynuclear Manganese Complexes with the Dicarboxylate Ligand *m*-Phenylenedipropionate: A Hexanuclear Mixed-Valence ($3Mn^{III}$, $3Mn^{IV}$) Complex

Cristina Cañada-Vilalta,[†] William E. Streib,[†,‡] John C. Huffman,[†] Ted A. O'Brien,[§] Ernest R. Davidson,[†,||] and George Christou*[,†,⊥]

Department of Chemistry and the Molecular Structure Center, Indiana University, Bloomington, Indiana 47405-7102, Department of Chemistry, Indiana University-Purdue University—Indianapolis, Indianapolis, Indiana 46202-3274, and Department of Chemistry, University of Florida, Gainesville, Florida 32611-7200

Received August 15, 2003

The dicarboxylate group *m*-phenylenedipropionate ($mpdp^{2-}$) has been used for the synthesis of four new Mn compounds of different nuclearities and oxidation states: $[Mn_2O(mpdp)(bpy)_2(H_2O)(MeCN)](ClO_4)_2$ (**3**), $[Mn_3O(mpdp)_3(py)_3](ClO_4)$ (**4**), $[Mn_3O(mpdp)_3(py)_3]$ (**5**), and $[Mn_6O_7(mpdp)_3(bpy)_3](ClO_4)$ (**6**). Compound **3** ($2Mn^{III}$) contains a $[Mn_2(\mu\text{-}O)]^{4+}$ core, whereas **5** (Mn^{II}, $2Mn^{III}$) and **4** ($3Mn^{III}$) contain the $[Mn_3(\mu_3\text{-}O)]^{6+,7+}$ core, respectively. In all three compounds, the $mpdp^{2-}$ ligand is flexible enough to adopt the sites occupied by two monocarboxylates in structurally related compounds, without noticeable distortion of the cores. Variable-temperature magnetic susceptibility studies establish that **3** and **5** have ground-state spin values of $S = 0$ and $S = 1/2$, respectively. Compound **6** is a highly unusual $3Mn^{III}$, $3Mn^{IV}$ trapped-valent compound, and it is also a new structural type, with six Mn atoms disposed in a distorted trigonal antiprismatic topology. Its electronic structure has been explored by variable-temperature measurements of its dc magnetic susceptibility, magnetization vs field response, and EPR spectrum. The magnetic data indicate that it possesses an $S = 3/2$ ground state with an axial zero-field splitting parameter of $D = -0.79$ cm^{-1}, and this conclusion is supported by the EPR data. The combined results demonstrate the ligating flexibility of the $mpdp^{2-}$ ligand and its usefulness in the synthesis of a variety of Mn_x species.

Introduction

We have a continuing strong interest in the development of new synthesis routes to polynuclear manganese species with oxide and carboxylate ligation.[1] This interest derives from their relevance to two fields. First, the ability of Mn to exist in a number of oxidation states (II−IV) under normal conditions has resulted in this metal being at the active sites of several redox enzymes, the most important of which is the water-oxidizing complex (WOC) on the donor side of photosystem II in green plants and cyanobacteria. The WOC comprises a tetranuclear Mn cluster, whose exact structure is still unclear, and is responsible for the light-driven, oxidative coupling of two molecules of water into dioxygen.[2,3] Second, polynuclear Mn compounds containing Mn^{III} have been found to often have large, and sometimes abnormally large, ground-state spin values (*S*), which combined with a large and negative magnetoanisotropy have led to some of

* Author to whom correspondence should be addressed. E-mail: christou@chem.ufl.edu.
† Indiana University.
‡ Deceased June 2002.
§ Indiana University-Purdue University—Indianapolis.
|| Current address: Department of Chemistry, University of Washington, Seattle, WA 98195-1700.
⊥ University of Florida.

(1) (a) Li, Q.; Vincent, J. B.; Chang, H. R.; Huffman, J. C.; Boyd, P. D. W.; Christou, G.; Libby, E.; Hendrickson, D. N. *Angew. Chem., Int. Ed. Engl.* **1988**, *27*, 1731. (b) Libby, E.; Webb, R. J.; Streib, W. E.; Folting, K.; Huffman, J. C.; Christou, G. *J. Chem. Soc., Chem. Commun.* **1989**, 1411. (c) Wang, S.; Folting, K.; Streib, W. E.; Schmitt, E. A.; McCusker, J. K.; Hendrickson, D. N.; Christou, G. *Angew. Chem., Int. Ed. Engl.* **1991**, *30*, 305. (d) Aromí, G.; Aubin, S. M. J.; Bolcar, M. A.; Christou, G.; Eppley, H. J.; Folting, K.; Hendrickson, D. N.; Huffman, J. C.; Squire, R. C.; Tsai, H. L.; Wang, S.; Wemple, M. W. *Polyhedron* **1998**, *17*, 3005 and references therein. (e) Cañada-Vilalta, C.; Huffman, J. C.; Christou, G. *Polyhedron* **2001**, *20(15−16)*, 1785. (f) Sañudo, E. C.; Grillo, V. A.; Knapp, M. J.; Bollinger, J. C.; Huffman, J. C.; Hendrickson, D. N.; Christou, G. *Inorg. Chem.* **2002**, *41(9)*, 2441.
(2) Law, N. A.; Caudle, M. T.; Pecoraro, V. L. In *Advances in Inorganic Chemistry*; Sykes, A. G., Ed.; Academic Press: London, 1998; Vol. 46, p 305.
(3) Yocum, C. F.; Pecoraro, V. L. *Curr. Opin. Chem. Biol.* **1999**, *3*, 182.

10.1021/ic034973m CCC: $27.50
Published on Web 12/12/2003

these species being able to function as single-molecule magnets (SMMs). These are individual molecules that behave as magnetizable magnets below a certain ("blocking") temperature.[4] Thus, they represent a molecular route to nanoscale magnetic materials.

As a result of the above, we have explored and successfully developed many new routes for the synthesis of polynuclear Mn complexes, with metal nuclearities currently up to 30. These procedures have included comproportionation reactions of simple starting materials,[2a] aggregation of clusters of smaller nuclearity,[5] fragmentation of higher nuclearity clusters,[6] and electrochemical oxidation,[7] disproportionation,[8] or ligand substitution of preformed species,[1e] among others.

A potentially powerful but barely explored route to new manganese compounds is the use of dicarboxylate ligands in place of the traditional monocarboxylate ligands. The advantages of dicarboxylates include (i) the possibility of triggering aggregation of preformed species into new, higher nuclearity products and (ii) the possible diversion of known reaction systems developed using monocarboxylates to new species as a result of the lower flexibility of dicarboxylates. Previous work along these lines has involved the use of phthalate ($phth^{2-}$) and 2,2-diethylmalonate (Et_2mal), and these successfully afforded the new high-nuclearity compounds $[Mn_{18}O_{16}(O_2CPh)_{22}(phth)_2(H_2O)_4]^{4-}$,[3c] $[Mn_{10}(OH)_3(phth)_9(bpy)_6]^-$,[4b] and $[Mn_8O_4(O_2CPh)_{12}(Et_2mal)_2(H_2O)]^{2-}$.[9]

The dicarboxylic acid *m*-phenylenedipropionic acid ($mpdpH_2$) is attractive for the above applications. It has been known in organic chemistry for a long time,[10] but its uses to date in coordination chemistry have been very few. Its

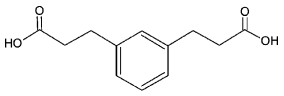

$mpdpH_2$

previous uses in this field are limited to a Rh_2 dimer with catalytic applications[11] and a dinuclear Fe^{III}_2 compound of interest for the modeling of protein active sites containing Fe−O−Fe units such as hemerythrin.[12] Our own work with this ligand has now led to the preparation of four new compounds: $[Mn_2O(mpdp)(bpy)_2(H_2O)(MeCN)](ClO_4)_2$ (**3**), $[Mn_3O(mpdp)_3(py)_3](ClO_4)$ (**4**), $[Mn_3O(mpdp)_3(py)_3]$ (**5**), and $[Mn_6O_7(mpdp)_3(bpy)_3](ClO_4)$ (**6**), the latter with an unprecedented hexanuclear Mn_6 topology and structure. The syntheses, structures, and physical properties of these species are described, as well as a particularly convenient new synthesis of the $mpdpH_2$ molecule.

Experimental Section

Syntheses. All manipulations were performed under aerobic conditions using chemicals as received, unless otherwise stated. $NBu^n_4MnO_4$,[13] $[Mn_2O(O_2CMe)_2(bpy)_2(H_2O)_2](ClO_4)_2$ (**1**),[14] and $[Mn_3O(O_2CMe)_6(py)_3](ClO_4)$ (**2**)[13] were prepared as described in the literature; bpy = 2,2′-bipyridine.

1,3-Bis(2-carbomethoxyethenyl)benzene. A solution of 1,3-dibromobenzene (10.2 mL, 84.8 mmol) in dry MeCN (80 mL) and Et_3N (60 mL) under an Ar atmosphere was treated with $Pd(O_2CMe)_2$ (0.373 g, 1.66 mmol) and tri-(*o*-tolyl)phosphine (1.02 g, 3.34 mmol). The mixture was stirred, and methyl acrylate (16.5 mL, 182.8 mmol) was added under reflux. After 2 h, the mixture was treated further with methyl acrylate (8.3 mL, 91.4 mmol), $Pd(OAc)_2$ (0.187 g, 0.83 mmol), and tri-(*o*-tolyl)phosphine (0.508 g, 1.67 mmol). The reflux was maintained overnight, and then the mixture was allowed to cool to room temperature. Water (55 mL) was added, and the resultant slurry was stirred for 10 min and then filtered, yielding a gray solid that was washed with copious water and hexanes and dried in air. Yield: 96%.

1,3-Bis(2-carbomethoxyethyl)benzene. A solution of 1,3-bis-(2-carbomethoxyethenyl)benzene (10.0 g, 40.7 mmol) in dry THF (250 mL) was treated with 5% Pd/C (1.36 g). The mixture was purged with Ar and then treated with an excess of H_2 gas. After an overnight reaction time, the system was purged with Ar and filtered over Celite. The filtrate was concentrated in vacuo to give a white solid. Yield: 83%.

***m*-Phenylenedipropionic Acid ($mpdpH_2$).** NaOH (8.0 g, 0.20 mmol) in H_2O (75 mL) was added to a solution of 1,3-bis(2-carbomethoxyethyl)benzene (8.3 g, 33 mmol) in MeOH (120 mL), and the mixture was stirred for several hours. The solution was concentrated in vacuo to approximately one-quarter its initial volume and treated with concentrated HCl until the pH was approximately 1. The resultant white precipitate was collected by filtration, extracted into ethyl acetate (1 × 100 mL, 3 × 25 mL), and filtered and the solvent removed in vacuo, giving the pure, white product in 93% yield. Anal. Calcd (Found) for $C_{12}H_{14}O_4$: C, 64.85 (64.62); H, 6.35 (6.38).

$[Mn_2O(mpdp)(bpy)_2(H_2O)(MeCN)](ClO_4)_2$ (3). Method A. Solid $mpdpH_2$ (0.147 g, 0.660 mmol) was added to a stirred dark brown solution of complex **1** (0.475 g, 0.600 mmol) in MeCN (25 mL). After 8 h, toluene (10 mL) was added, and the mixture was rotary-evaporated to dryness. The resulting solid was redissolved in MeCN (20 mL) and toluene (5 mL), and the solution was again rotary-evaporated to dryness to give a gray solid. This was collected by filtration and washed with Et_2O to remove the excess acid. The product was dissolved in MeCN (15 mL), the solution filtered, and

(4) (a) Lis, T. *Acta Crystallogr., Sect. B* **1980**, *36*, 2042. (b) Soler, M.; Chandra, S. K.; Ruiz, D.; Huffman, J. C.; Hendrickson, D. N.; Christou, G., *Polyhedron* **2001**, *20*, 1279. (c) Aubin, S. M. J.; Sun, Z.; Eppley, H. J.; Rumberger, E. M.; Guzei, I. A.; Folting, K.; Gantzel, P.; Rheingold, A. L.; Christou, G.; Hendrickson, D. N. *Polyhedron* **2001**, *20*, 1139.
(5) (a) Wang, S.; Huffman, J. C.; Folting, K.; Streib, W. E.; Lobkovsky, E.; Christou, G. *Angew. Chem., Int. Ed. Engl.* **1991**, *30*, 1672. (b) Tsai, L.; Wang, S.; Folting, K.; Streib W. E.; Hendrickson, D. N.; Christou, G. *J. Am. Chem. Soc.* **1995**, *11*, 7, 2503. (c) Squire, R. C.; Aubin, S. M. J.; Folting, K.; Streib, W. E.; Christou, G.; Hendrickson, D. N. *Inorg. Chem.* **1995**, *34*, 6463.
(6) (a) Bhaduri, S.; Tasiopoulos, A.; Pink, M.; Abboud, K. A.; Christou, G. *Chem. Commun.* **2002**, 2352. (b) Cañada-Vilalta, C.; Pink, M.; Christou, G. *J. Chem. Soc., Dalton Trans* **2003**, 1121.
(7) Aliaga, N.; Folting, K.; Hendrickson, D. N.; Christou, G. *Polyhedron* **2001**, *20*, 1273.
(8) Perlepes, S. P.; Huffman, J. C.; Christou, G. *J. Chem. Soc., Chem. Commun.* **1991**, *23*, 1657.
(9) Wemple, M. W.; Tsai, H.-L.; Wang, S.; Claude, J. P.; Streib, W. E.; Huffman, J. C.; Hendrickson, D. N.; Christou, G. *Inorg. Chem.* **1996**, *35*, 6437.
(10) Schimelpfenig, C. W. *J. Org. Chem.* **1975**, *40*, 1493.
(11) Taber, D. F.; Meagley, R. P.; Louey, J. P.; Rheingold, A. L. *Inorg. Chim. Acta* **1995**, *239*, 25.
(12) Beer, R. H.; Tolman, W. B.; Bott, S. G.; Lippard, S. J. *Inorg. Chem.* **1991**, *30(9)*, 2082.
(13) Vincent, J. B.; Chang, H.-R.; Folting, K.; Huffman, J. C.; Christou, G.; Hendrickson, D. N. *J. Am. Chem. Soc.* **1987**, *109*, 5703.
(14) Vincent, J. B.; Tsai, H. L.; Blackman, A. G.; Wang, S.; Boyd, P. D. W.; Folting, K.; Huffman, J. C.; Lobkovsky, E. B.; Hendrickson, D. N.; Christou, G. *J. Am. Chem. Soc.* **1993**, *115*, 12353.

the filtrate layered with Et_2O (20 mL). After several days, the resultant black crystals were collected by filtration, washed with Et_2O, and dried in air. The yield was 74%. Anal. Calcd (Found) for **1**·H_2O, $C_{34}H_{35}N_5O_{15}Cl_2Mn_2$: C, 43.71 (43.51); H, 3.78 (3.95); N, 7.50 (7.16). $[Mn_2O(mpdp)(4,4'\text{-}Me_2bpy)_2(H_2O)(MeCN)](ClO_4)_2$ (**3′**) was prepared in an analogous manner using 4,4′-dimethylbipyridine for use in the NMR studies.

Method B. A solution of $Mn(ClO_4)_2$·$6H_2O$ (0.145 g, 0.400 mmol) in MeCN (20 mL) was treated successively with solid bpy (78 mg, 0.50 mmol), $mpdpH_2$ (56 mg, 0.25 mmol), and $NBu^n_4ClO_4$ (34 mg, 0.10 mmol). The resultant yellow solution was treated dropwise with a solution of $NBu^n_4MnO_4$ (36 mg, 0.10 mmol) in MeCN (3 mL), and it slowly turned dark brown. After a further 5 min, the solution was filtered and the filtrate concentrated to half its initial volume to initiate crystallization. Small black crystals were obtained over a few hours. These were collected by filtration, washed with a little MeCN, and dried in air. The yield was 56%, based on the total available Mn. The product was spectroscopically identical (by IR) with material from method A.

$[Mn_3O(mpdp)_3(py)_3](ClO_4)$ (4). A dark brown solution of **2** (2.00 g, 2.29 mmol) in MeCN (150 mL) was treated with solid $mpdpH_2$ (1.53 g, 6.88 mmol) and stirred for several hours. Toluene (20 mL) was added and the solution then rotary-evaporated to dryness. The residue was redissolved in MeCN (100 mL), toluene (20 mL) added, and the solution rotary-evaporated to dryness. This process was repeated four times, giving the product in 73% yield. Recrystallization from CH_2Cl_2/Et_2O gave black crystals. Anal. Calcd (Found) for **2**·$^1/_2CH_2Cl_2$, $C_{51.5}H_{52}N_3O_{17}Cl_2Mn_3$: C, 50.68 (50.84); H, 4.29 (4.17); N, 3.44 (3.32).

$[Mn_3O(mpdp)_3(py)_3]$ (5). Method A. $NBu^n_4MnO_4$ (27 mg, 0.075 mmol) in MeCN (5 mL) was added dropwise to a solution of **4** (0.20 g, 0.16 mmol) in MeCN (25 mL). The solvent was removed by rotary evaporation, and the resulting brown solid was slurried in CH_2Cl_2, collected by filtration, washed with CH_2Cl_2, and dissolved in pyridine (7 mL). The solution was filtered and the filtrate layered with Et_2O (6 mL). After several days, the resultant black crystals were collected by filtration, washed with Et_2O, and dried in air. The yield was 7%. The material was spectroscopically identical with that from method C.

Method B. A solution of **4** (0.20 g, 0.16 mmol) in MeCN (20 mL) was treated with triethylamine (3 mL), and air was bubbled through it overnight. This produced a brown precipitate that was collected by filtration and dissolved in pyridine (5 mL). The solution was filtered and layered with Et_2O (5 mL) to produce black crystals in 6% yield. The material was spectroscopically identical with that from method C.

Method C. A solution of **4** (100 mg) in pyridine (8 mL) was treated with an equal volume of Et_2O and left to stand undisturbed at room temperature. After 3 weeks, the black platelike crystals that had formed were collected by filtration, washed with Et_2O, and dried. The yield was 73%. Anal. Calcd (Found) for **5**·$^1/_2H_2O$·$^1/_2$py, $C_{53.5}H_{53.5}N_{3.5}O_{13}Mn_3$: C, 57.46 (57.39); H, 4.82 (4.84); N, 4.38 (4.56).

Method D. $NBu^n_4ClO_4$ (45 mg, 0.13 mmol) dissolved in pyridine (2 mL) was added slowly to a solution of $Mn(OAc)_2$·$4H_2O$ (0.20 g, 0.81 mmol) and $mpdpH_2$ (0.21 g, 0.94 mmol) in pyridine (8 mL). The mixture was stirred for 15 min and then filtered to remove some dark brown precipitate. Addition of Et_2O to the filtrate produced a gray precipitate, which was collected by filtration, washed with Et_2O, and dried in air. The yield was 25%. The material was spectroscopically identical with that from method C.

$[Mn_6O_7(mpdp)_3(bpy)_3](ClO_4)$ (6). Method A. $NBu^n_4MnO_4$ (18 mg, 0.050 mmol) dissolved in MeCN (3 mL) was added dropwise to an essentially black solution of **3** (0.115 g, 0.125 mmol) in MeCN (20 mL). The color changed immediately to dark brown. The solution was filtered and the filtrate allowed to stand undisturbed at room temperature for several weeks, during which time small, well-formed, black crystals grew. They were collected by filtration, washed with a little MeCN, and dried in air. The yield was 8%. Anal. Calcd (Found) for **6**·$^1/_2$MeCN, $C_{67}H_{61.5}N_{6.5}O_{23}Mn_6Cl$: C, 47.60 (46.81); H, 3.67 (3.56); N, 5.39 (5.47).

Method B. A solution of **4** (0.40 g, 0.33 mmol) in MeCN (25 mL) was treated successively with solid bpy (87 mg, 0.56 mmol) and a solution of $NBu^n_4MnO_4$ (50 mg, 0.14 mmol) in MeCN (5 mL), added dropwise. The resultant dark brown solution was stirred for an additional 5 min and filtered to eliminate any remaining solid and the filtrate allowed slowly to concentrate by slow evaporation. Black crystals were obtained after several weeks, and they were isolated by filtration. The yield was 10%. The identity of this material was confirmed by spectroscopic comparison (NMR, IR) with that from method A.

X-ray Crystallography and Solution of Structures. Crystallographic data were collected on a SMART 6000 (Bruker) diffractometer. Suitable crystals were attached to the tip of a glass capillary using silicone grease and transferred to the goniostat, where they were cooled for characterization and data collection, using Mo Kα radiation (graphite monochromator). The structures were solved using a combination of direct methods (SHELXL-97[15]) and Fourier techniques. Data collection parameters and structure solution details are listed in Table 1.

Complex **3**·3MeCN crystallizes in the triclinic space group $P\bar{1}$, with the Mn_2 cation, two perchlorate anions, and three MeCN molecules in the asymmetric unit. Non-hydrogen atoms were refined with anisotropic displacement parameters. Hydrogen atoms were placed in fixed, idealized positions for the final cycles of refinement, and they were refined as riding atoms with isotropic displacement parameters related to those of the parent atoms. The final full-matrix least-squares refinement on F converged to $R = 0.0486$, $R_w = 0.0506$ ($I > 2\sigma(I)$). The final difference Fourier map was essentially featureless, the largest peak being 0.99 e/A^3.

Complex **4** crystallizes in the monoclinic space group $P2_1/c$, with the asymmetric unit containing the trinuclear cation and a perchlorate anion. Non-hydrogen atoms were refined with anisotropic displacement parameters. A difference Fourier map phased on the non-hydrogen atoms located many of the hydrogen atoms, but since their positions could be readily calculated, they were treated as fixed atom contributors in the final least-squares refinement cycles. Thus, hydrogen atoms were placed in fixed idealized positions and refined as riding atoms with isotropic displacement parameters related to those of the parent atoms. The final full-matrix least-squares refinement on F converged to $R = 0.0349$, $R_w = 0.0273$ ($I > 2\sigma(I)$).

Complex **5**·py crystallizes in the monoclinic space group $P2_1/c$, with two independent molecules in the asymmetric unit, as well as two py molecules (rotationally disordered and refined as benzenes). The two molecules are essentially related by a translation of 1/2 along the *a* axis, which resulted in a "supercell" in the initial data reduction. Although the structure was solvable using the supercell model, the solution obtained had significant disorder in one ligand and large thermal parameters for many of the other atoms. When the proper cell was utilized, the two independent molecules became apparent. In both cases, there is one Mn atom (Mn3) whose chemical environment is substantially different from those of the other two. The presence of two independent molecules indicates

(15) SHELXTL-Plus V5. 10, Bruker Analytical X-ray Systems, Madison, WI.

Table 1. Crystallographic Data for **3**·3MeCN, **4**, **5**·2C_6H_6, and **6**·3.5MeCN

	3·3MeCN	**4**	**5**·2C_6H_6	**6**·3.5MeCN
empirical formula	$C_{40}H_{42}Cl_2Mn_2N_8O_{14}$	$C_{51}H_{51}ClMn_3N_3O_{17}$	$C_{57}H_{57}Mn_3N_3O_{13}$	$C_{51}H_{51}ClMn_3N_3O_{17}$
fw	1039.6	1178.24	1156.91	1178.24
cryst color, size (mm^3)	brown, 0.30 × 0.25 × 0.25	orange, 0.10 × 0.34 × 0.34	black, 0.3 × 0.2 × 0.12	orange, 0.10 × 0.34 × 0.34
temp (K)	98	117(2)	113(2)	117(2)
wavelength (Å)	0.71073	0.71073	0.71073	0.71073
cryst syst, space group	triclinic, $P\bar{1}$	monoclinic, $P2_1/c$	monoclinic, $P2_1/c$	monoclinic, $P2_1/c$
unit cell dimens	a = 11.4924(4) Å, α = 83.056(1)°	a = 16.099(4) Å, α = 90°	a = 16.6348(4) Å, α = 90°	a = 16.099(4) Å, α = 90°
	b = 12.4571(4) Å, β = 74.937(1)°	b = 13.216(2) Å, β = 96.748(4)°	b = 32.4251(8) Å, β = 111.8298°	b = 13.216(2) Å, β = 96.748(4)°
	c = 16.5064(6) Å, γ = 74.937(1)°	c = 24.497(5) Å, γ = 90°	c = 20.6235(5) Å, γ = 90°	c = 24.497(5) Å, γ = 90°
vol ($Å^3$)	2250.28(14)	5176.0(18)	10326.3(4)	7885.0(5)
Z	2	4	8	4
density(calcd) (g/cm^3)	1.534	1.512	1.488	1.528
abs coeff (mm^{-1})	0.7544	0.8473	0.7923	1.046
abs correctn	semiemp from equivalents	semiemp from equivalents	semiemp from equivalents	semiemp from equivalents
no. of data/ params	78930/596	4287/677	10371/1369	34959/1972
GOF	1.9855[a]	0.6111[a]	0.6741[a]	0.968[c]
final R indices (obsd data)	R1 = 0.0486,[b] wR2 = 0.0506	R1 = 0.0349,[b] wR2 = 0.0293	R1 = 0.0336,[b] wR2 = 0.0390	R1 = 0.0674,[d] wR2 = 0.1585[e] [$I > 2\sigma(I)$]
R indices (all data)				R1 = 0.1029,[d] wR2 = 0.1847[e]
largest diff peak and hole ($e/Å^3$)	1 and −1.15	0.58 and −0.4	0.54 and −0.43	1.467 and −0.883

[a] Goodness of fit on F. [b] $R1 = \sum(|F_o| - |F_c|)/\sum|F_o|$. [c] Goodness of fit on $F^2 = [\sum[w(F_o^2 - F_c^2)^2]/N_{observns} - N_{params})]^{1/2}$, all data. [d] $R1 = \sum(|F_o| - |F_c|)/\sum|F_o|$. [e] $wR2 = [\sum[w(F_o^2 - F_c^2)^2]/\sum[w(F_o^2)^2]]^{1/2}$.

that this asymmetry is inherent to the molecule and not merely due to packing effects. All non-hydrogen atoms were refined with anisotropic displacement parameters. All hydrogen atoms were located, and they were placed in fixed positions for the final cycles of refinement on F. The final full-matrix least-squares refinement converged to $R = 0.0336$, $R_w = 0.0332$ ($I > 2\sigma(I)$), and the final Fourier difference map was essentially featureless.

Complex **6**·3.5MeCN crystallizes in the monoclinic space group $P2_1$. Each unit cell includes two asymmetric units, and each asymmetric unit contains two enantiomeric cations, two ClO_4^- anions, and seven MeCN molecules. The structure is a racemic mixture, with two types of cations that are idealized mirror images of each other but that are not related by symmetry within the cell. The crystal was refined as a twin, with the twin law matrix −1 0 0, 0 1 0, 0 0 1. The fractional contribution of the minor component of the twin refined to 0.29. Restraints were used on two of the distances in the perchlorate anions, and the thermal parameters on the perchlorate oxygen atoms were fixed at a large average value. Most hydrogen atoms were included as riding atoms; six hydrogen atoms on two Me groups of the solvent molecules were fixed. All non-hydrogen atoms were refined with anisotropic displacement parameters. The full-matrix least-squares refinement on F^2 converged to $R_w(F^2) = 0.185$ for the 1972 total variables; $R(F) = 0.067$ for 23926 data points ($F_o > 4\sigma(F_o)$), and $R(F) = 0.103$ for all 34959 data. The above twin law matrix, however, indicates that the minor component has the inverse absolute structure. The largest peak in the final difference Fourier map was 1.47 $e/Å^3$ in the vicinity of one of the perchlorate anions, and the deepest hole was −0.88 $e/Å^3$.

Other Studies. Infrared spectra were recorded in the solid state (KBr pellets) on a Nicolet model 510P FTIR spectrophotometer in the 400−4000 cm^{-1} range. ^1H and ^2H NMR spectra were obtained in CD_3CN solution with a 300 MHz Varian Gemini 2000 NMR spectrometer, with the solvent protio signal as reference. Elemental analyses (C, H, N) were performed on a Perkin-Elmer 2400 series II. Cyclic and differential pulse voltammograms were recorded at room temperature on a BAS CV50W voltammetric analyzer using a glassy carbon working electrode, a Pt wire auxiliary electrode, and an SCE reference electrode. The supporting electrolyte was $NBu^n_4PF_6$, and the solvent was distilled MeCN. Magnetic measurements were performed on a Quantum Design MPMS-XL SQUID magnetometer equipped with a 7 T magnet at Indiana University. Pascal's constants were used to estimate the diamagnetic correction, which was subtracted from the experimental susceptibility to give the molar magnetic susceptibility (χ_M). EPR measurements were performed at X-band frequencies (9.4 GHz) on a Bruker ESP300D spectrometer with a Hewlett-Packard 5350B microwave frequency counter.

Results and Discussion

Syntheses. The synthesis of $mpdpH_2$ as reported in the literature involves the condensation of isophthalaldehyde and malonic acid in a Döbner synthesis,[16,17] followed by hydrogenation of the product.[8] In the present work, however, 1,3-dibromobenzene has been used as the starting material for a convenient three-step synthesis that produces the final dicarboxylic acid in a very high yield. The process was adapted from that reported for the 1,3,5-trisubstituted analogue:[18] 1,3-Dibromobenzene was first treated with methyl acrylate in the presence of palladium acetate, tri(*o*-tolyl)phosphine, and triethylamine (Heck reaction) to give 1,3-benzenediacrylate, which was then hydrogenated with H_2 gas using Pd/C as a catalyst. Finally, the resulting diester was saponified to give the diacid $mpdpH_2$.

The initial strategy explored for the incorporation of $mpdpH_2$ into manganese complexes was a carboxylate

(16) Gensler, W. J.; Bernam, E. *J. Am. Chem. Soc.* **1958**, *80*, 4949.
(17) Ziegler, K.; Luttringhaus, A.; Liebigs, J. *Ann. Chem.* **1934**, *511*, 1.
(18) Majchrzak, M. W.; Zobel, J. N.; Obradovich, D. J.; Peterson, G. A. *OPPI Briefs* **1997**, *29*, 361.

substitution reaction on preformed acetate-containing Mn_x clusters. This procedure proved to be very successful for the conversion in MeCN of $[Mn_2O(OAc)_2(bpy)_2(H_2O)_2](ClO_4)_2$ (**1**) and $[Mn_3O(OAc)_6(py)_3](ClO_4)$ (**2**) into $[Mn_2O(mpdp)(bpy)_2(MeCN)(H_2O)](ClO_4)_2$ (**3**) and $[Mn_3O(mpdp)_3(py)_3](ClO_4)$ (**4**), respectively. In both cases, the conversion involves the stoichiometric reaction with $mpdpH_2$, with the resulting equilibrium driven to completion by removal of acetic acid under vacuum as its azeotrope with toluene (28% AcOH/72% toluene, bp 105°). The reactions are summarized in eqs 1 and 2.

$$[Mn_2O(OAc)_2(bpy)_2(H_2O)_2]^{2+} + mpdpH_2 + MeCN \rightleftharpoons [Mn_2O(mpdp)(bpy)_2(MeCN)(H_2O)]^{2+} + 2AcOH + H_2O \quad (1)$$

$$[Mn_3O(OAc)_6(py)_3]^{+} + 3mpdpH_2 \rightleftharpoons [Mn_3O(mpdp)_3(py)_3](ClO_4) + 6AcOH \quad (2)$$

An alternative, direct, and therefore more convenient synthesis of complex **4** involves the comproportionation of $Mn(ClO_4)_2$ and $NBu^n_4MnO_4$ in MeCN, in the presence of stoichiometric amounts of bpy and $mpdpH_2$. This is summarized in eq 3 The same product is obtained even if the

$$8Mn^{2+} + 2MnO_4^- + 10bpy + 5mpdpH_2 + 5MeCN + 2H_2O \rightarrow 5[Mn_2O(mpdp)(bpy)_2(MeCN)(H_2O)]^{2+} + 4H^+ \quad (3)$$

proportions of the Mn reagents vary significantly from those in eq 3, as long as the amount of $mpdpH_2$ is not in excess, or insoluble precipitates will form, probably polymeric species. The addition of $NBu^n_4ClO_4$ to the reaction solution increases the concentration of counterion and facilitates crystallization of the product.

$[Mn_3O(mpdp)_3(py)_3]$ (**5**) was obtained from several reactions and crystallized readily from py/Et_2O layerings. Thus, treatment of **4** in MeCN with reagents such as atmospheric O_2 or $NBu^n_4MnO_4$ followed by recrystallization from pyridine/Et_2O yields compound **5**. In fact, when compound **4** is recrystallized in this solvent system, the product is **5** in very good yield, suggesting that all these reaction systems yield complicated disproportionation and other equilibria from which preferential crystallization of **5** occurs. A more rational synthesis of compound **5** involves the air oxidation of $Mn(OAc)_2$ in pyridine containing $mpdpH_2$ and $NBu^n_4ClO_4$. A precipitate containing mostly NBu^n_4OAc was separated by filtration, and compound **5** was obtained from the filtrate on addition of Et_2O.

$[Mn_6O_7(mpdp)_3(bpy)_3](ClO_4)$ (**6**) was originally obtained during attempts to oxidize dinuclear complex **3** to a $Mn^{III}Mn^{IV}$ product. The treatment of **3** with 1 equiv of $K_2S_2O_8$ in MeCN gave a precipitate containing no carboxylate, and its IR spectrum was very similar to that of known $[Mn^{III}Mn^{IV}O_2(bpy)_4](ClO_4)_3$,[19] suggesting the product was likely the analogous complex with sulfate as the anion. However, with permanganate as the oxidizing agent, a very different result was obtained. Treatment of 5 equiv of **3** with 2 equiv of $NBu^n_4MnO_4$ in MeCN led to the formation of small black crystals of the new hexanuclear cluster **6** in low yield (eq 4). This compound has an average metal oxidation

$$3MnO_4^- + 12[Mn_2O(mpdp)(bpy)_2(H_2O)(MeCN)]^{2+} \rightarrow 4[Mn_6O_7(mpdp)_3(bpy)_3]^{+} + 12bpy + 12MeCN + 8H_2O + 8H^+ + 3Mn^{3+} \quad (4)$$

state of +3.5 and an unprecedented structure (vide infra). Its formation can be rationalized by the higher affinity of Mn^{IV}, a hard acid, compared with Mn^{III} for hard bases such as oxide. Thus, when compound **3** is oxidized, its $[Mn_2(\mu\text{-}O)(\mu\text{-}O_2CR)_2]^{2+}$ core, typical of $2Mn^{III}$ dinuclear complexes, will convert to a $[Mn_2(\mu\text{-}O)_2(\mu\text{-}O_2CR)]^{2+}$ one, characteristic of $Mn^{III}Mn^{IV}$ and $2Mn^{IV}$ complexes. This requires one of the carboxylate arms of the bridging $mpdp^{2-}$ group to be displaced, allowing it to bridge to another unit and facilitating formation of a higher nuclearity product. The net result is the rearrangement of three dinuclear units to form compound **6**.

With the identity of **6** established, an alternative synthetic route was developed involving the oxidation of **4** with $NBu^n_4MnO_4$ in the presence of bpy (eq 5). Many attempts

$$3MnO_4^- + 7[Mn_3O(mpdp)_3(py)_3]^{+} + 12bpy + 9H_2O \rightarrow 4[Mn_6O_7(mpdp)_3(bpy)_3]^{+} + 21py + 9mpdpH_2 \quad (5)$$

to prepare **6** directly by a comproportionation reaction using different ratios of $NBu^n_4MnO_4$, $mpdpH_2$, bpy, $NBu^n_4ClO_4$, and different sources of manganese (e.g., $Mn(ClO_4)_2$ and $Mn(OAc)_2$) instead resulted in either the dinuclear compound **3** or insoluble precipitates, presumably containing polymeric species. Thus, both successful methods to **6** are low yield (≤10%), but at least they are reproducible and give clean material for further study.

Description of Structures. An ORTEP representation of the cation of complex **3** is presented in Figure 1. Selected bond distances and angles are listed in Table 2. The cation consists of two hexacoordinated Mn^{III} atoms bridged by a μ-oxide ion and two μ-carboxylate units from the ligand $mpdp^{2-}$. Each Mn ion is additionally ligated by a chelating bpy and a MeCN or H_2O group. The latter is hydrogen-bonded to the two ClO_4^- anions ($d(O\cdots O) = 2.77-2.86$ Å), and this is likely the origin of the asymmetry in the molecule in the solid state; most of the related dinuclear units reported in the literature contain the same ligand at the two terminal positions.[12,20] The Mn ions exhibit a marked Jahn−Teller (JT) distortion, as expected for high-spin d^4 Mn^{III} ions in near-octahedral geometry. Each ion has three statistically nonequivalent axes, the shortest one passing through the central μ-oxide atom and the other two through carboxylate

(19) (a) Plaksin, P. M.; Stoufer, R. C.; Matthew, M.; Palenik, G. J. *J. Am. Chem. Soc.* **1972**, *94*, 212. (b) Wilson, C.; Larsen, F. K.; Figgis, B. N. *Acta Crystallogr., Sect. C* **1998**, *54*, 1797.

(20) Sheats, J. E.; Czernuszewicz, R. S.; Dismukes, G. C.; Rheingold, A. L.; Petrouleas, V.; Stubbe, J.; Armstrong, W. H.; Beer, R. H.; Lippard, S. J. *J. Am. Chem. Soc.* **1987**, *109*, 1435.

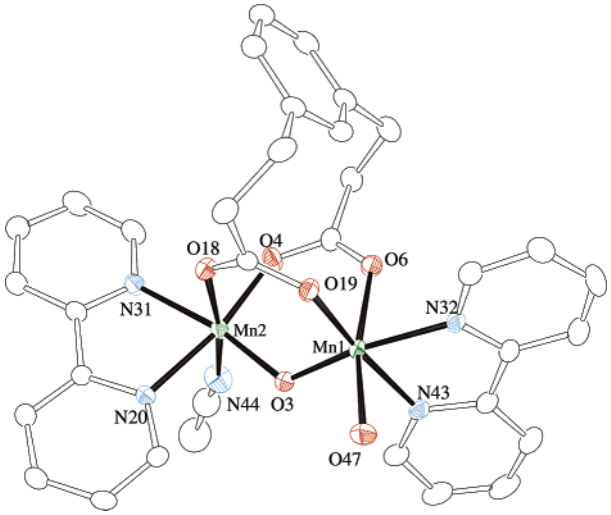

Figure 1. Labeled ORTEP representation of the cation of **3** at the 50% probability level. Hydrogen atoms have been omitted for clarity.

Table 2. Selected Interatomic Distances (Å) and Angles (deg) for Compound **3**

Distances

Mn1	Mn2	3.139(1)	Mn2	O18	2.1766(18)
Mn1	O3	1.7844(17)	Mn2	N20	2.0749(19)
Mn1	O6	2.1348(16)	Mn2	N31	2.0657(21)
Mn1	O19	1.9704(16)	Mn2	N44	2.2760(23)
Mn1	O47	2.2324(18)	O4	C5	1.2835(28)
Mn1	N32	2.0696(20)	O6	C5	1.245(3)
Mn1	N43	2.0628(19)	O18	C17	1.247(3)
Mn2	O3	1.7895(17)	O19	C17	1.2864(27)
Mn2	O4	1.9614(16)			

Angles

Mn1	O3	Mn2	122.88(9)	O3	Mn2	O4	100.42(7)
O3	Mn1	O6	96.26(7)	O3	Mn2	O18	94.36(7)
O3	Mn1	O19	98.70(7)	O3	Mn2	N20	90.73(8)
O3	Mn1	O47	96.28(7)	O3	Mn2	N31	169.13(8)
O3	Mn1	N32	169.15(8)	O3	Mn2	N44	94.67(9)
O3	Mn1	N43	90.81(8)	O4	Mn2	O18	90.09(7)
O6	Mn1	O19	91.67(6)	O4	Mn2	N20	168.85(8)
O6	Mn1	O47	167.45(7)	O4	Mn2	N31	90.45(8)
O6	Mn1	N32	83.79(7)	O4	Mn2	N44	89.70(8)
O6	Mn1	N43	93.15(7)	O18	Mn2	N20	89.41(7)
O19	Mn1	O47	87.00(7)	O18	Mn2	N31	86.06(8)
O19	Mn1	N32	92.14(7)	O18	Mn2	N44	170.86(8)
O19	Mn1	N43	168.81(8)	N20	Mn2	N31	78.40(8)
O47	Mn1	N32	83.79(7)	N20	Mn2	N44	89.03(8)
O47	Mn1	N43	86.11(7)	N31	Mn2	N44	84.80(9)
N32	Mn1	N43	78.37(8)				

oxygen atoms. There are two sets of Mn−O(carboxylate) distances, 1.961(2)/1.970(2) and 2.135(2)/2.177(2) Å, respectively. The first pair corresponds to the oxygen atoms *trans* to bpy and the second to the oxygen atoms *trans* to the H_2O and MeCN molecules, which also have long bonds to the Mn ions. Thus, the axes containing the latter groups define JT elongation axes.

The bpy ligands are disposed in a near-perpendicular fashion. This is also the case for the JT axes, as reflected in the torsion angle O(H_2O)−Mn1−Mn2−N(MeCN) of 98.6°. This and other structural parameters are typical of dinuclear complexes with a $[Mn_2(\mu\text{-O})(\mu\text{-O}_2CR)_2]^{2+}$ core (Table 3). The dihedral angle between the least-squares planes formed by the five atoms of each bridging carboxylate unit (i.e., Mn1−O6−C5−O4−Mn2 and Mn1−O19−C17−O18−Mn2) is 87.4°, comparable to that in complexes with two bridging monocarboxylate groups, e.g., 85.1° in $[Mn_2O(OAc)_2(bpy)_2(H_2O)_2](ClO_4)_2$ and 89.3° in $[Mn_2O(O_2CPh)_2(bpy)_2(N_3)_2]$. These results underscore the great flexibility of the dicarboxylate ligand $mpdp^{2-}$, which is accommodated in the dinuclear unit without causing any significant distortion compared with complexes with two monocarboxylate bridging groups.

An ORTEP representation of the cation of complex **4** is presented in Figure 2, and selected bond distances and angles are listed in Table 4. The cation consists of three Mn^{III} atoms in a triangular arrangement, connected by a central μ_3-oxide. Two carboxylate groups from the same $mpdp^{2-}$ ligand bridge each pair of Mn ions, and a terminal pyridine group completes octahedral coordination at each Mn. The cation has no crystallographic symmetry. The Mn−O distances and angles involving Mn ions are also statistically nonequivalent, and therefore, the structure can be accurately described as scalene. The Mn ions are Jahn−Teller elongated, with the elongation axes containing the oxygen atoms of the carboxylate groups. The structure is very similar to those observed for similar $[Mn_3O]^{7+}$ complexes with monocarboxylate ligands,[21] which again demonstrates that the dicarboxylate ligand is flexible enough to replace two monocarboxylates without causing significant distortions.

A labeled ORTEP plot of **5** is shown in Figure 3, and selected bond distances and angles are listed in Table 5. The structure is very similar to that of **4**. It consists of a triangular array of three Mn atoms connected by a central μ_3-oxide ion, with an $mpdp^{2-}$ group bridging each Mn_2 pair and a terminal pyridine on each Mn. The Mn−μ_3-O distances are 1.858 and 1.827 Å for Mn1 and Mn2, respectively, and 2.097 Å for Mn3. This and the other bond distances at the latter Mn clearly demonstrate that Mn3 is Mn^{II}, and that the complex is trapped-valence Mn^{II}, $2Mn^{III}$. The molecule has no crystallographic symmetry and can be described as a scalene triangle, as is **4**. Mn1 and Mn2 are both Jahn−Teller distorted, with the elongation axes passing through carboxylate O atoms. Once again, the structural parameters of **5** are similar to those for analogous compounds but with monocarboxylate ligands.[6]

A labeled ORTEP representation and a stereoview of **6** are shown in Figure 4. Table 6 lists selected distances and angles. The crystal structure consists of a racemic mixture, with two enantiomeric cations not related by symmetry within the asymmetric unit. Figure 4 shows one of the two isomers, which are structurally very similar, and Table 6 lists selected structural parameters for the same one.

The $[Mn_6O_7]$ core of the cation, shown separately in Figure 5, comprises six Mn atoms disposed in a distorted trigonal antiprismatic topology. There are two triangular Mn_3 subunits disposed in a face-to-face, nearly staggered arrangement, with a noncrystallographic C_3 axis perpendicular to both and

(21) (a) Vincent, J. B.; Cheng, H.-R.; Folting, K.; Huffman, J. C.; Christou, G.; Hendrickson, D. N. *J. Am. Chem. Soc.* **1987**, *109*, 5703. (b) An, J.; Chen, Z.-D.; Bian, J.; Jin, X.-L.; Wang, S.-X.; Xu, G.-X. *Inorg. Chim. Acta* **1999**, *287*, 82. (c) Li, J.; Yang, S.; Zhang, F.; Tang, Z.; Ma, S.; Shi, Q.; Wu, Q.; Huang, Z. *Inorg. Chim. Acta* **1999**, *294*, 109.

Table 3. Selected Crystallographic and Magnetic Data on $[Mn^{III}_2(\mu\text{-}O)(\mu\text{-}O_2CR)_2]^{2+}$ Complexes

complex	J (cm^{-1})	d(Mn···Mn) (Å)	∠(Mn···O···Mn) (deg)	ref
$[Mn_2O(OAc)_2(Me_3TACN)_2]^{2+}$	9	3.15	120.9	35
$[Mn_2O(OAc)_2(HB(pz)_3)_2]$	<−0.2	3.159	125.1	36
$[Mn_2O(O_2CPh)_2(bpy)_2(N_3)_2]$	8.8	3.153	122.0	14
$[Mn_2O(O_2CPh)_2(bpy)_2(OH)(NO_3)]$	1	3.141	124.1	26
$[Mn_2O(OAc)_2(TMIP)_2]^{2+}$	−0.2 to −0.7	3.164	124.4	37
$\{[Mn_2O(OAc)_2(bbpm)]^{2+}\}_2$	−0.4	3.261	118.5	38
$[Mn_2O(mpdp)(bpy)_2(MeCN)(H_2O)]^{2+}$	−0.6	3.139	122.9	a
$[Mn_2O(OAc)_2(bpy)_2(H_2O)_2]^{2+}$	−3.4	3.152	122.7	14
$[Mn_2O(OAc)_2(bpy)_2Cl_2]$	−4.1	3.153	124.3	14

[a] This work.

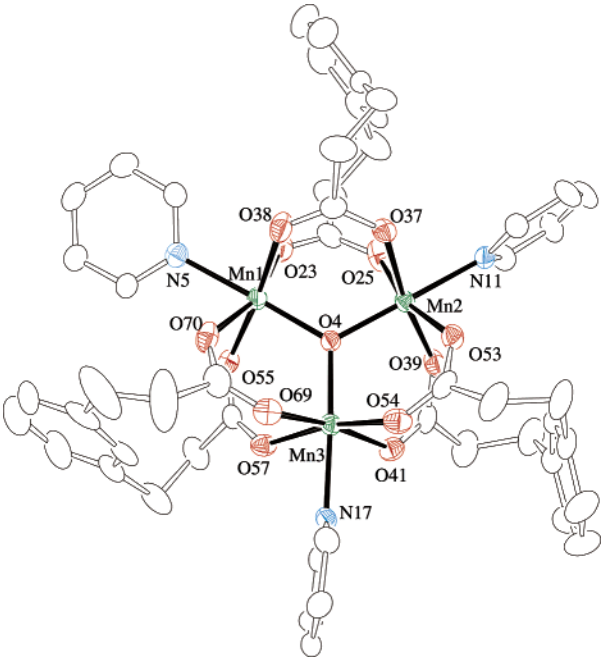

Figure 2. Labeled ORTEP representation of the cation of **4** at the 50% probability level. Hydrogen atoms have been omitted for clarity.

passing through O13. The lower Mn_3 fragment (below the dashed line in Figure 5) is a $[Mn^{IV}_3(\mu\text{-}O)_3]^{6+}$ nonplanar hexagonal ring in a chair conformation, while the upper fragment is a cuboidal $[Mn^{III}_3(\mu\text{-}O)_4]^{+}$ unit, three of whose O atoms bridge the two fragments and thus become μ_3. The three remaining coordination positions at the Mn^{IV} centers are occupied by two N atoms from a chelating bpy and by an O atom from a bridging carboxylate, which also binds to a Mn^{III} ion in the neighboring Mn_3 unit. The three remaining positions at the Mn^{III} centers are occupied by bridging carboxylate groups: two bridge Mn^{III} pairs, and the third bridges a Mn^{III}/Mn^{IV} pair. Each Mn^{III}−OCO−Mn^{III} bridge is linked to a Mn^{III}−OCO−Mn^{IV} bridge through a phenyl ring.

The three high-spin Mn^{III} ions exhibit clear JT axial elongation, with the bonds on one of the axes being considerably longer than those on the other two axes, even though the ligands are identical for all three axes (a μ_3-O^{2-} atom and a carboxylate O atom in each case). Each JT axis thus contains one of the μ_3-O^{2-} ions on the open triangular face of the cuboidal unit and the *trans* carboxylate group. As a result, the open triangular face of the $[Mn^{III}_3(\mu_3\text{-}O)_4]^{+}$ cuboidal unit has alternating long and short Mn−O^{2-} bonds. For example,

Table 4. Selected Interatomic Distances (Å) and Angles (deg) for Compound **4**

Distances

Mn1	Mn2	3.275(2)	Mn2	O37	2.002(4)
Mn1	Mn3	3.310(2)	Mn2	O39	1.976(5)
Mn2	Mn3	3.274(2)	Mn2	O53	2.076(5)
Mn1	O4	1.898(4)	Mn2	N11	2.077(5)
Mn1	O23	2.033(5)	Mn3	O4	1.905(4)
Mn1	O38	2.072(5)	Mn3	O41	2.071(5)
Mn1	O55	2.073(5)	Mn3	O54	1.990(5)
Mn1	O70	2.028(5)	Mn3	O57	2.008(5)
Mn1	N5	2.072(5)	Mn3	O69	2.070(5)
Mn2	O4	1.888(4)	Mn3	N17	2.091(5)
Mn2	O25	2.104(5)			

Angles

O4	Mn1	O23	100.3(2)	O25	Mn2	N11	80.9(2)
O4	Mn1	O38	92.7(2)	O37	Mn2	O39	172.8(2)
O4	Mn1	O55	92.2(2)	O37	Mn2	O53	85.5(2)
O4	Mn1	O70	96.9(2)	O37	Mn2	N11	87.8(2)
O4	Mn1	N5	178.2(2)	O39	Mn2	O53	93.1(2)
O23	Mn1	O38	90.0(2)	O39	Mn2	N11	85.0(2)
O23	Mn1	O55	87.8(2)	O53	Mn2	N11	85.4(2)
O23	Mn1	O70	162.8(2)	O4	Mn3	O41	94.5(2)
O23	Mn1	N5	80.0(2)	O4	Mn3	O54	98.1(2)
O38	Mn1	O55	175.0(2)	O4	Mn3	O57	93.7(2)
O38	Mn1	O70	88.7(2)	O4	Mn3	O69	93.7(2)
O38	Mn1	N5	89.1(2)	O4	Mn3	N17	177.0(2)
O55	Mn1	O70	92.1(2)	O41	Mn3	O54	91.4(2)
O55	Mn1	N5	86.0(2)	O41	Mn3	O57	89.5(2)
O70	Mn1	N5	82.9(2)	O41	Mn3	O69	171.7(2)
O4	Mn2	O25	97.0(2)	O41	Mn3	N17	86.2(2)
O4	Mn2	O37	93.0(2)	O54	Mn3	O57	168.2(2)
O4	Mn2	O39	94.2(2)	O54	Mn3	O69	86.2(2)
O4	Mn2	O53	96.8(2)	O54	Mn3	N17	84.8(2)
O4	Mn2	N11	177.7(2)	O57	Mn3	O69	91.3(2)
O25	Mn2	O37	923.0(2)	O57	Mn3	N17	83.4(2)
O25	Mn2	O39	86.7(2)	O69	Mn3	N17	85.7(2)
O25	Mn2	O53	166.2(2)				

Mn6−O9 (2.209(8) Å) is considerably longer than Mn6−O11 (1.849(8) Å).

The flexibility of the $mpdp^{2-}$ ligand is evident in the structure of **6**, in which this ligand bridges two separate oxide-bridged Mn_2 pairs and in doing so adopts a twisted conformation; the latter is very different from that observed in the dinuclear and trinuclear compounds discussed above.

^{1}H NMR Spectroscopy of Complex 3. ^{1}H NMR studies of paramagnetic Mn^{III} complexes are rarely available in the literature, and a study of complex **3** has therefore been carried out in CD_3CN. The relative simplicity of this compound has allowed the assignment and interpretation of all the signals in its spectrum. This has been supplemented by a variable-temperature study to provide information about the dynamic behavior of the complex in solution.

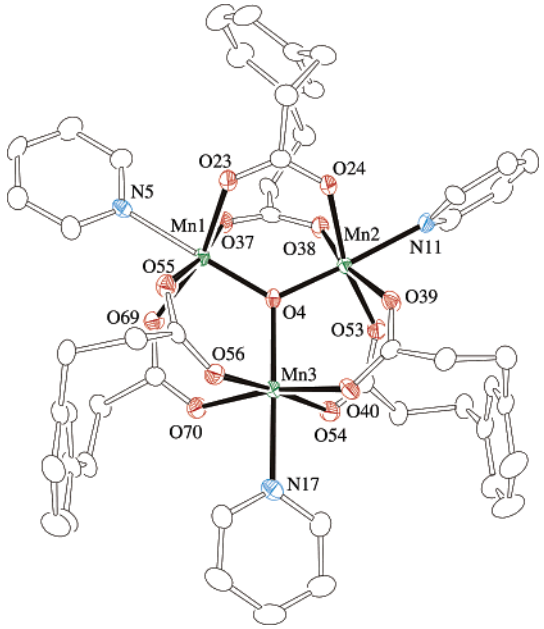

Figure 3. Labeled ORTEP representation of **5** at the 50% probability level. Hydrogen atoms have been omitted for clarity.

Table 5. Selected Interatomic Distances (Å) and Angles (deg) for Compound **5**

Distances

Mn1	O4	1.858(4)	Mn2	O39	2.039(4)
Mn1	O23	2.016(4)	Mn2	O53	2.104(4)
Mn1	O37	2.127(4)	Mn2	N11	2.104(5)
Mn1	O55	2.152(4)	Mn3	O4	2.097(4)
Mn1	O69	2.024(4)	Mn3	O40	2.123(4)
Mn1	N5	2.116(5)	Mn3	O54	2.178(4)
Mn2	O4	1.827(4)	Mn3	O56	2.188(4)
Mn2	O24	2.089(4)	Mn3	O70	2.123(4)
Mn2	O38	2.061(4)	Mn3	N17	2.256(5)

Angles

O4	Mn1	O23	98.3 (2)	O4	Mn2	O38	96.9(2)
O4	Mn1	O37	92.7(2)	O4	Mn2	O39	96.2(2)
O4	Mn1	O55	96.2(2)	O4	Mn2	O53	99.1(2)
O4	Mn1	O69	97.5 (2)	O4	Mn2	N11	173.8(2)
O4	Mn1	N5	177.9 (2)	O24	Mn2	O38	90.0(2)
O23	Mn1	O37	91.4(2)	O24	Mn2	O39	92.6(2)
O23	Mn1	O55	86.9 (2)	O24	Mn2	O53	164.9(2)
O23	Mn1	O69	163.9(2)	O24	Mn2	N11	80.1(2)
O23	Mn1	N5	81.6(2)	O38	Mn2	O39	166.4(2)
O37	Mn1	O55	171.2(2)	O38	Mn2	O53	82.1(2)
O37	Mn1	O69	90.9(2)	O38	Mn2	N11	86.4(2)
O37	Mn1	N5	85.3(2)	O39	Mn2	O53	92.2(2)
O55	Mn1	O69	88.5(2)	O39	Mn2	N11	80.9(2)
O55	Mn1	N5	85.9(2)	O53	Mn2	N11	86.5(2)
O69	Mn1	N5	82.7(2)	O4	Mn3	O40	98.0(2)
O4	Mn2	O24	94.7(2)	O4	Mn3	O54	92.7(2)
O54	Mn3	O70	90.9(2)	O70	Mn3	N17	84.5(2)
O54	Mn3	N17	85.9(2)	Mn1	O4	Mn2	123.4(2)
O56	Mn3	O70	89.5(2)	Mn1	O4	Mn3	120.0(2)
O56	Mn3	N17	89.4(2)	Mn2	O4	Mn3	116.6(2)

The ^{1}H NMR spectrum of **3** is shown in Figure 6, and Table 7 lists the corresponding chemical shifts. The spectrum displays broad, paramagnetically shifted resonances spread over a wide chemical shift range of +54 to −118 ppm. Nevertheless, it was possible to assign all the signals on the basis of their isotropic shifts, line widths, and peak integrations, together with measurements at different temperatures and comparison with the ^{1}H and ^{2}H NMR spectra of analogous compounds.

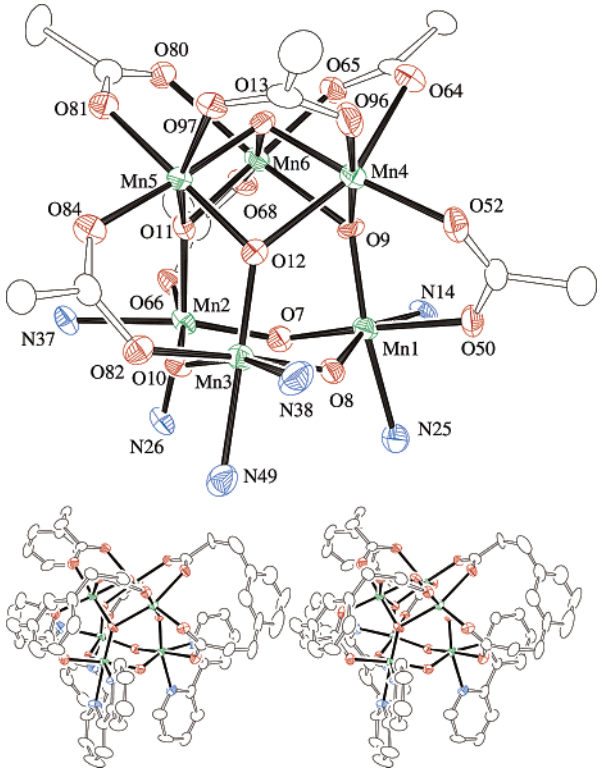

Figure 4. Labeled ORTEP representation of the cation of **6**, with bpy and mpdp^{2-} aromatic rings omitted (top), and an ORTEP stereopair of the complete cation from the same viewpoint (bottom). The figures are at the 50% probability level, and hydrogen atoms have been omitted for clarity.

The resonances due to the H_b, H_c, H_d, and H_e hydrogen nuclei of the mpdp^{2-} ligand were identified by comparison of the ^{1}H spectrum of **3** with that of $[Mn_2O(OAc)_2(bpy)_2(H_2O)_2](ClO_4)_2$ (**7**). These are the only signals that appear

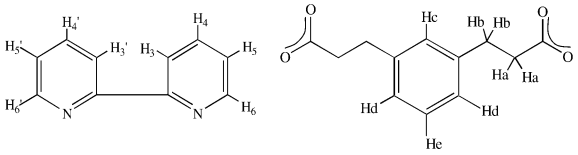

in the spectrum of **3** but not in that of **7**. In contrast, the resonances due to the bpy groups appear in the same regions for both compounds. The same is true for the signal from the CH_2 hydrogen atoms, H_a, which have a chemical environment very similar to that of the Me hydrogen atoms of the acetate groups in **7**. The assignments of the H_b, H_c, H_d, and H_e signals were then made on the basis of their integrations and line widths. The broadness of a peak is proportional to r^{-6}, where r is the distance between the resonating nucleus and the paramagnetic center.[22] The average Mn···H distances in the solid state are 5.3 Å for H_b, 6.6 Å for H_d, and 7.1 Å for H_e. On this basis, the three peaks at 5.2, 6.8, and 7.7 ppm are assigned to H_b, H_e, and H_d, respectively, which is also consistent with their respective integrations (4:1:2). The remaining proton H_c is only about 3.5 Å from the Mn nuclei, so it should be considerably broader. Consequently, the low, broad band at 13 ppm is

(22) Drago, R. S. *Physical Methods for Chemists*, 2nd ed.; Saunders College Publishing: Mexico, 1992; p 523.

Table 6. Selected Interatomic Distances (Å) and Angles (deg) for Compound **6**

Distances

Mn1	Mn2	3.268(4)	Mn2	N37	2.137(10)
Mn1	Mn3	3.259(3)	Mn3	O8	1.756(7)
Mn1	Mn4	3.201(3)	Mn3	O10	1.812(7)
Mn1	Mn5	4.556(3)	Mn3	O12	1.765(8)
Mn1	Mn6	3.611(4)	Mn3	O82	2.018(8)
Mn2	Mn3	3.286(3)	Mn3	N38	2.171(11)
Mn2	Mn4	4.606(3)	Mn3	N49	2.179(11)
Mn2	Mn5	3.623(4)	Mn4	O9	1.865(8)
Mn2	Mn6	3.185(4)	Mn4	O12	2.224(8)
Mn3	Mn4	3.651(3)	Mn4	O13	1.867(8)
Mn3	Mn5	3.208(4)	Mn4	O52	1.994(9)
Mn3	Mn6	4.564(3)	Mn4	O64	2.248(9)
Mn4	Mn5	2.951(3)	Mn4	O96	1.923(9)
Mn4	Mn6	2.938(3)	Mn5	O11	2.168(8)
Mn5	Mn6	2.901(5)	Mn5	O12	1.902(8)
Mn1	O7	1.802(8)	Mn5	O13	1.876(9)
Mn1	O8	1.842(7)	Mn5	O81	1.966(10)
Mn1	O9	1.764(8)	Mn5	O84	1.955(8)
Mn1	O50	2.007(9)	Mn5	O97	2.203(9)
Mn1	N14	2.081(10)	Mn6	O9	2.209(8)
Mn1	N25	2.131(11)	Mn6	O11	1.849(8)
Mn2	O7	1.801(9)	Mn6	O13	1.854(8)
Mn2	O10	1.794(7)	Mn6	O65	1.988(8)
Mn2	O11	1.809(8)	Mn6	O68	1.948(9)
Mn2	O66	2.003(9)	Mn6	O80	2.227(10)
Mn2	N26	2.078(10)			

Angles

O7	Mn1	O8	98.9(4)	O12	Mn4	O96	85.2(3)
O7	Mn1	O9	93.3(4)	O13	Mn4	O52	175.6(4)
O7	Mn1	O50	170.5(4)	O13	Mn4	O64	81.3(3)
O7	Mn1	N14	90.4(4)	O13	Mn4	O96	91.6(4)
O7	Mn1	N25	86.6(4)	O52	Mn4	O64	94.5(3)
O8	Mn1	O9	104.2(3)	O52	Mn4	O96	89.9(4)
O8	Mn1	O50	88.3(3)	O64	Mn4	O96	95.2(3)
O8	Mn1	N14	159.0(4)	Mn1	O7	Mn2	130.2(5)
O8	Mn1	N25	88.5(4)	Mn1	O8	Mn3	129.9(4)
O9	Mn1	O50	90.8(4)	Mn1	O9	Mn4	123.7(4)
O9	Mn1	N14	93.9(4)	Mn1	O9	Mn6	130.3(4)
O9	Mn1	N25	167.1(4)	Mn4	O9	Mn6	91.9(3)
O50	Mn1	N14	80.7(4)	Mn2	O10	Mn3	131.3(4)
O50	Mn1	N25	87.4(4)	Mn2	O11	Mn5	131.0(4)
N14	Mn1	N25	73.2(4)	Mn2	O11	Mn6	121.0(4)
O9	Mn4	O12	89.7(3)	Mn5	O11	Mn6	92.1(3)
O9	Mn4	O13	85.9(3)	Mn3	O12	Mn4	132.2(4)
O9	Mn4	O52	92.9(4)	Mn3	O12	Mn5	122.0(4)
O9	Mn4	O64	89.1(3)	Mn4	O12	Mn5	91.0(3)
O9	Mn4	O96	174.7(4)	Mn4	O13	Mn5	104.1(4)
O12	Mn4	O13	77.7(3)	Mn4	O13	Mn6	104.3(4)
O12	Mn4	O52	106.5(3)	Mn5	O13	Mn6	102.1(4)
O12	Mn4	O64	159.0(3)				

assigned to H_c. Among the remaining peaks, those of diastereotopic H_a and $H_{a'}$ were assigned to the resonances at 25.7 and 51.2 ppm. This is consistent with the large paramagnetic shifts expected for these hydrogen atoms, and the assignment was confirmed by the variable-temperature studies (vide infra).

The bpy resonances were assigned with the aid of $[Mn_2O(mpdp)(4,4'\text{-}Me_2bpy)_2(H_2O)(MeCN)](ClO_4)_2$ (**3′**). Its ^{1}H NMR spectrum is essentially identical with that of **3** except that the resonances at ∼−33 ppm are replaced by Me resonances at ∼46 ppm. The former signals are thus the resonances due to the H_4 and $H_{4'}$ hydrogen atoms. The H_6 and $H_{6'}$ hydrogens are the closest to the Mn (3.1 Å vs 4.9−5.8 Å for the other bpy hydrogens) and are consequently the most paramagnetically broadened. They are thus assigned to the broad resonances at ∼−115 ppm. The two remaining peaks are due to the bpy *meta* hydrogen atoms ($H_3/H_{3'}$ and $H_5/H_{5'}$), but it is not possible to unequivocally distinguish these signals with our presently available data. Note that isotropic shifts that are both negative and positive (i.e., paramagnetic shifts both upfield and downfield) for nuclei in the same aromatic ring are typical of contact shifts in an aromatic system from a π-delocalization mechanism.[23]

The H_2O resonance at ∼11 ppm in Figure 6 is the exchange-weighted average of bound and free H_2O and thus

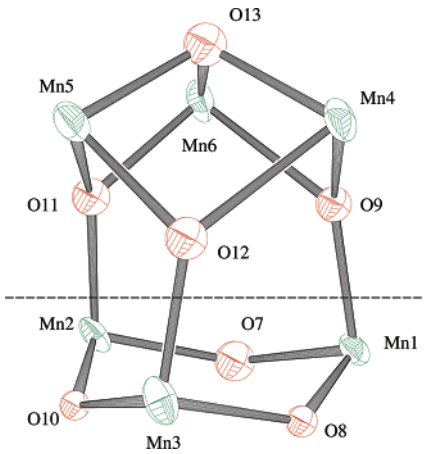

Figure 5. Labeled ORTEP representation of the $[Mn_6O_7]$ core of the cation of complex **6**. The dashed line shows its dissection into the two subunits discussed in the text.

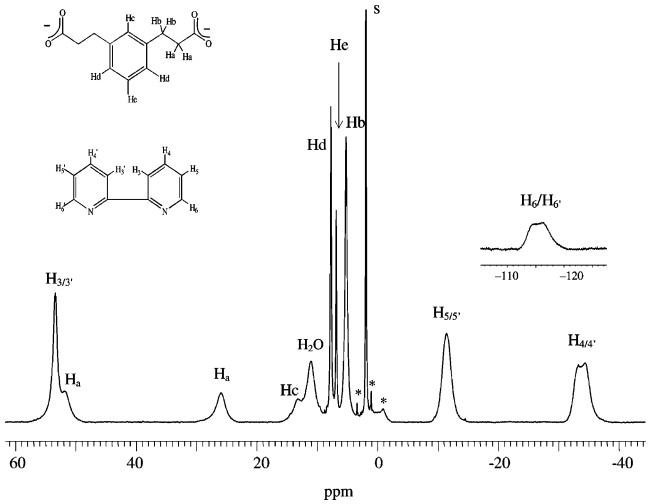

Figure 6. ^{1}H NMR spectrum of complex **3** in CD_3CN.

Table 7. ^{1}H NMR Data[a] for Compounds **3** and **3′**

3		**3′**	
chemical shift (ppm)	assignment	chemical shift (ppm)	assignment
∼−116	H_6/H_6	∼−115	H_6/H_6
∼−33	H_4/H_4	45.8	CH_3bpy
∼−11	H_5/H_5	∼−11	H_5/H_5
5.2	H_b	5.2	H_b
6.8	H_e	6.8	H_e
7.7	H_d	7.7	H_d
∼13	H_c	∼13	H_c
∼26, ∼52	H_a	∼26, nr	H_a
∼54	H_3/H_3	∼52	H_3/H_3

[a] In acetonitrile at ∼20 °C; nr = not resolved.

(23) Wemple, M. H.; Tsai, H.-L.; Folting, K.; Hendrickson, D. N.; Christou, G. *Inorg. Chem.* **1993**, *32*, 2025.

has been seen to vary in its position (between 4 and 15 ppm) depending on the concentration of the complex and the water content of the NMR solvent used.

Variable-temperature ^{1}H NMR studies on complex **3** were performed to probe any dynamic processes and confirm the above assignments. The spectra were recorded from −20 to +74 °C and are provided as Supporting Information. Even assuming fast exchange of bound and free solvent molecules, as seems very likely especially given their location on JT elongation axes, the cation of **3** should still possess C_1 solution symmetry because of the orientation of the mpdp^{2-} phenylene ring. It should thus exhibit 16 bpy resonances and 12 from the mpdp^{2-} ligand, 8 of them from diastereotopic CH_2 groups; however, significantly fewer signals are seen in the spectra. This is indicative of higher effective solution symmetry due to fluxional processes. The VT spectra show that, at temperatures below room temperature, eight bpy resonances become frozen out, indicating an inequivalence between the two halves of each bpy group but equivalence of the two separate bpy groups. Similarly, raising the temperature broadens the bpy signals, and eventually they coalesce and sharpen. The diastereotopic H_a and $H_{a'}$ resonances also broaden at higher temperature and eventually coalesce at 70 °C, and this is particularly informative. It is clear that two fluxional processes must be invoked to explain the observed spectra.

First, the very flexible mpdp^{2-} can very likely swivel rapidly, during which it passes through a position in which its phenylene ring is oriented perpendicular to the Mn···Mn axis. Assuming the H_2O and MeCN groups are exchanging rapidly, this will generate a C_2 symmetry axis in the molecule that will relate the two bpy groups and also the two halves of the dicarboxylate ligand. This would result in a total of fifteen signals, eight from the two equivalent bpy ligands and seven from the mpdp^{2-} group, three of which (H_c, H_d, H_e) are from the phenylene ring and four from the two pairs of diastereotopic methylene protons (H_a and $H_{a'}$, H_b and $H_{b'}$).

However, the NMR spectrum shows coalescence of diastereotopic methylene resonances at higher temperatures, and an additional dynamic process must therefore be invoked. This is almost certainly the rotational rocking of the bpy groups, which could be facilitated by loss of bound solvent and generation of five-coordinate Mn intermediates. At positions at which the bpy groups are parallel to each other (rather than perpendicular as in the crystal structure), vertical mirror planes are introduced (one bisecting the bpy groups), and in combination with the swiveling of the mpdp^{2-} group, the effective solution symmetry of the cation becomes C_{2v}. This makes the two halves of each bpy equivalent, resulting in only four bpy signals, and the diastereotopic methylene hydrogens of mpdp^{2-} also become equivalent. Every pair of H and H′ peaks would thus coalesce into one signal, and only nine resonances would be observed. This is consistent with the observed high-temperature spectra.

An intermediate situation is observed at room temperature, in which some pairs of peaks have coalesced and others have not, particularly the resonances from the H_a and $H_{a'}$ hydrogens; a temperature of 70 °C is needed for these signals to coalesce. Conversely, by decreasing the temperature to −20 °C, the exchange of the $H_3/H_{3'}$, $H_4/H_{4'}$, and $H_6/H_{6'}$ pairs can be frozen out.

Determining the temperature of coalescence of the well-separated H_a and $H_{a'}$ resonances allows the lifetime of the two interconverting states A and B to be calculated. At coalescence, eq 6 applies,[24] where τ is the lifetime of each

$$2\pi(\Delta\nu)\tau = \sqrt{2} \tag{6}$$

state and $\Delta\nu$ ($= \nu_A - \nu_B$) is the frequency separation between the two resonances in the absence of exchange. In diamagnetic systems, chemical shifts are essentially temperature independent and the $\Delta\nu$ in the slow exchange region can be used to calculate the rate of exchange. In paramagnetic systems, however, the population of the spin states follows a Boltzmann distribution and thus changes with temperature. This changes the effective net spin on the molecules, which varies the effective magnetic field on the nuclei and strongly influences the isotropic shift. Consequently, a measurement of the chemical shift difference at low temperature does not give the value corresponding to that at the coalescence temperature, as it would for diamagnetic systems. For this reason, $\Delta\nu$ was extrapolated from the variation observed before the coalescence process began. This was carried out for the H_a and $H_{a'}$ resonances assuming a Curie behavior ($\Delta\nu = c/T$) as the extrapolating expression. This gave $\Delta\nu =$ 6505 Hz (21.7 ppm) at the temperature of coalescence (70 °C). Using this value in eq 6 gives a lifetime of $\tau = 3.46 \times 10^{-5}$ s. This value was employed in the Eyring relationship[24] (eq 7) to get an estimate of the activation energy, where k, h, and R are the Boltzmann, Planck, and gas constants, respectively. The calculated activation free energy was 13.3 ± 0.4 kcal mol^{-1} for the fluxional process involving the bpy groups.

$$\tau^{-1} = \frac{kT}{h}\exp\left(\frac{-\Delta G^{\ddagger}}{RT}\right) \tag{7}$$

Analogous calculations were performed with the complex $[Mn_2O(mpdp)(4,4'\text{-}Me_2bpy)_2(H_2O)(MeCN)](ClO_4)_2$, this time using the coalescence of the methyl resonances of the 4,4′-Me_2bpy ligand. The two peaks merge at 20 °C, and the extrapolated value of $\Delta\nu$ for this temperature is 670 Hz (2.3 ppm). This yields a value of τ of 3.36×10^{-4} s and a resulting activation free energy of 12.5 ± 0.5 kcal mol^{-1}. As expected, the values obtained for the fluxional process are very similar for the two compounds, since they only differ in the substituents on the bpy rings.

Magnetochemistry. Variable-temperature dc magnetic susceptibility data were measured for complexes **3**, **5**, and **6** on powdered, microcrystalline samples in the 5.00−300 K range in an applied magnetic field of 1 T. Since there are many previous magnetic studies on Mn_3 complexes, we did not study both **4** and **5** but only representative complex **5**.

For **3**, the effective magnetic moment (μ_{eff}) decreases only slightly with decreasing temperature from 6.7 μ_B at 300 K

(24) Drago, R. S. *Physical Methods for Chemists*, 2nd ed.; Saunders College Publishing: New York, NY, 1992.

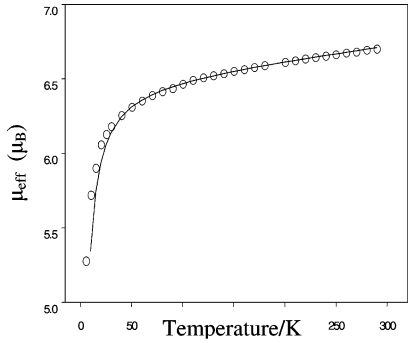

Figure 7. μ_{eff} vs T for complex **3**. The solid line is the fit of the data; see the text for the fit parameters.

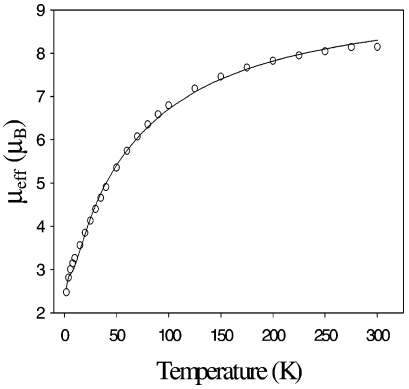

Figure 8. μ_{eff} vs T for compound **5**. The solid line is the fit of the data; see the text for the fit parameters.

to 6.3 μ_B at 40.0 K and then decreases more rapidly to 5.3 μ_B at 5.00 K (Figure 7); the 300 K value is essentially equal to that for two noninteracting $S = 2$ metal ions. This behavior is indicative of a pair of antiferromagnetically coupled, high-spin d^4 ions. The coupling is clearly very weak, and the compound thus deviates from Curie behavior only at very low temperatures. This makes difficult the fitting of the experimental data to an appropriate theoretical expression to obtain an accurate value of the exchange parameter, J, between the two metal atoms. The latter is so weak in this case that effects that are usually neglected, such as intermolecular interactions and zero-field splitting (ZFS), are very likely of comparable magnitude. Nevertheless, to obtain a rough estimate of J, the data were fit assuming the isotropic spin Hamiltonian given in eq 8. The theoretical μ_{eff} vs T

$$H = -2J_{12}\hat{S}_1 \cdot \hat{S}_2 \tag{8}$$

equation, derived using the Van Vleck equation and given elsewhere,[14] was used to fit the data. The fit parameters were $J_{12} = -0.58$ cm^{-1} and $g = 1.87$, with TIP $= 150 \times 10^{-5}$ cm^3 mol^{-1}, where TIP is the temperature-independent paramagnetism. The fit is shown as a solid line in Figure 7. While the values of g and J appear very reasonable, the TIP is about 4 times larger than is typical for a molecule with two high-spin Mn^{III} ions, no doubt due to the only approximate nature of the model employed. The only safe conclusion is that the exchange interaction in this complex is antiferromagnetic and very weak.

The above conclusion is consistent with the previously recognized fact that the exchange interaction is known to be very weak in complexes with the $[Mn^{III}_2O(O_2CR)_2]$ core. This weakness and, more generally, the relationship between magnetic interactions and structural properties in these compounds have been the objects of much discussion.[12,25−27] Table 3 lists the pertinent structural and magnetic parameters of those members of this family for which both types of data are available. J is always very small, ranging from +9 to −5.1 cm^{-1}. Since the observed J is the sum of ferromagnetic (J_F) and antiferromagnetic (J_{AF}) contributions and these are of comparable magnitude, its sign is sensitive to even small changes in the relative magnitudes of the latter. We have previously discussed the variation in the exchange parameter for a series of $[Mn_2O(OAc)_2(bpy)_2X_2]$ compounds,[14] where J is ferromagnetic for X = N_3^- and antiferromagnetic for X = Cl^- or H_2O. The terminal ligand X was concluded to be important because of its influence on the energy of the $d_{x^2-y^2}$ orbital (taking the z axis as along the Mn−oxide bond), which mediates antiferromagnetic Mn−Mn interactions via the carboxylate ligands. When X is the stronger field ligand azide, the energy of the $d_{x^2-y^2}$ orbital is raised, increasing the energy difference between it and the orbitals of the carboxylate bridge. Therefore, this antiferromagnetic contribution to the overall interaction is weaker than in the Cl^- or H_2O compounds, and the overall J parameter becomes positive. In the present case of compound **3**, the weak-field H_2O and MeCN terminal groups would suggest the J value should be negative (antiferromagnetic), and this is indeed what is observed.

For **5**, the μ_{eff} vs temperature plot is shown in Figure 8. The μ_{eff} value per Mn_3 decreases gradually with decreasing temperature from 8.14 μ_B at 300 K to a minimum of 2.48 μ_{eff} at 2.0 K. The 300 K value is slightly below that corresponding to a noninteracting Mn^{II}, $2Mn^{III}$ system, indicating the presence of antiferromagnetic exchange interactions. The data were fit to the theoretical expression derived elsewhere for a Mn^{II}, $2Mn^{III}$ isosceles triangle,[28] with J_A and J_B being the Mn^{II}−Mn^{III} and Mn^{III}−Mn^{III} interactions, respectively. The fit gave two fits of comparable quality: $J_A = -4.6(5)$ cm^{-1}, $J_B = -7.5(8)$ cm^{-1}, and $g = 1.89(5)$, and $J_A = -4.7$ (2) cm^{-1}, $J_B = -3.1(7)$ cm^{-1}, and $g = 1.83$-(1). In both cases, the TIP was held constant at 600×10^{-4} cm^{3}mol^{-1}. These two sets of values correspond to two different $S = 1/2$ ground states. Denoting the total spin of the Mn_3 system as S_T and the combination of the spins of the two Mn^{III} ions as S_A, the first fit gives the $|S_T, S_A\rangle = |1/2, 2\rangle$ ground state, with the first excited state being $|3/2,$

(25) Corbella, M.; Costa, R.; Ribas, J.; Fries P. H.; Latour, J. M.; Ohrström, L.; Solans, X. and Rodríguez, V. *Inorg. Chem.* **1996**, *35*, 1857.
(26) Hotzelmann, R.; Wieghardt, K.; Flörke, U.; Haupt, H.-J. Weatherburn, D. C.; Bonvoisin, J.; Blondin, G.; Girerd, J.-J. *J. Am. Chem. Soc.* **1992**, *114*, 1681.
(27) Hendrickson, D. N.; Christou, G.; Schmitt, E. A.; Libby, E.; Bashkin, J. S.; Wang, S.; Tsai, H. L.; Vincent, J. B.; Boyd, P. D. W. *J. Am. Chem. Soc.* **1992**, *114*, 2455.
(28) (a) Castro, S. L.; Streib, W. E.; Sun, J.-S.; Christou, G. *Inorg. Chem.* **1996**, *35*, 4462. (b) Karet, G. B.; Castro, S. L.; Folting, K.; Bollinger, J. C.; Heintz, R. A.; Christou, G. *J. Chem. Soc., Dalton Trans.* **1998**, 67.

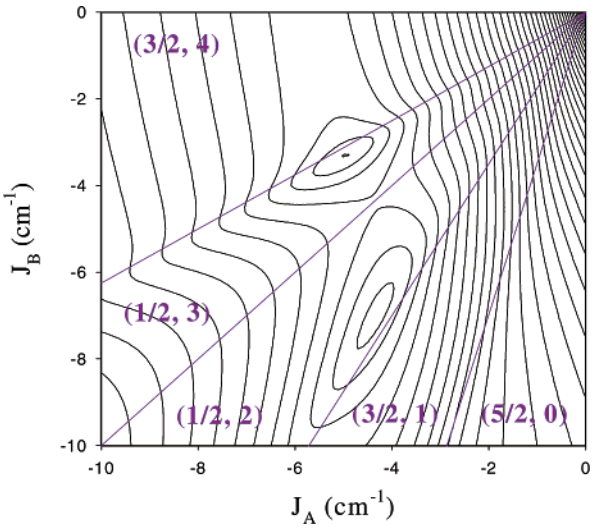

Figure 9. 2-D contour plot of the least-squares error surface of the magnetic susceptibility fit for **5** as a function of J_A and J_B. The straight lines define the boundaries between areas with different values of $|S_T, S_A\rangle$.

1⟩ only 2.2 cm^{-1} above the ground state. The second fit gives the $|1/2, 3\rangle$ ground state, with the first excited state being $|3/2, 4\rangle$ at only 1.3 cm^{-1}. The solid line in Figure 8 corresponds to the latter fit. The error surface for the fit (Figure 9), calculated using $g = 1.86$, clearly shows these two minima and, superimposed, the boundaries between different $|S_T, S_A\rangle$ ground-state regions as a function of the J_A/J_B ratio. Both minima lie very close to the boundaries between different ground states, i.e., a very-low-lying excited state.

The above are consistent with the expected presence of spin frustration in this complex:[29] there are two competing antiferromagnetic interactions, and it is impossible in this triangular arrangement for all spins to be aligned antiparallel to both their neighboring spins at the same time.[29] The resulting compromise (or balance) in the spin alignments (and thus the ground state of the molecule) depends greatly on the relative magnitude of the competing exchange interactions.

With the data fitting suggesting such a low-lying $S = 3/2$ state, we worried whether the true situation might be inverted, with an $S = 3/2$ ground state and an $S = 1/2$ low-lying excited state. To probe this, we carried out ac magnetic susceptibility studies. ac measurements are performed in the absence of an applied dc field, thus eliminating any complicating effects of the latter. In this compound, there is no out-of-phase ac signal (χ_M''), and thus, the in-phase signal (χ_M') will be essentially equal to the dc susceptibility. The obtained $\chi_M'T$ vs T plot is shown in Figure 10 and confirms the low value indicated by the dc data as not being due to Zeeman effects from the dc field. In addition, the ac data do not reach a plateau at low temperatures, indicating the presence of excited states so low in energy that they are populated even at these temperatures. Nevertheless, extrapolation of the $\chi_M'T$ curve to 0 K gives a value of ca. 0.4−0.5 cm^3 K mol^{-1}, close to the value expected for a doublet ground state (0.375 cm^3 K mol^{-1}) and very different from that for a spin quartet (1.875 cm^3 K mol^{-1}). Thus, the ac data support an $S = 1/2$ ground state for compound **5**.

(29) (a) Khan, O. *Chem. Phys. Lett.* **1997**, *265*, 109. (b) McCusker, J. K.; Jang, H. G.; Wang, S.; Christou, G.; Hendrickson, D. N. *Inorg. Chem.* **1992**, *31*, 1874.

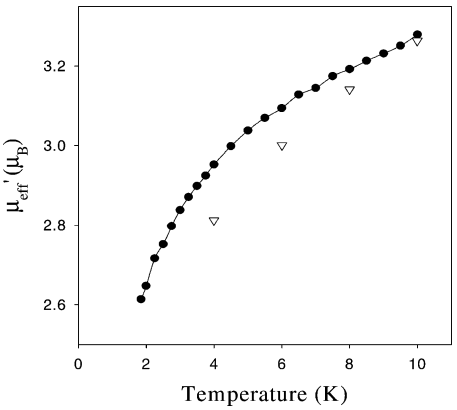

Figure 10. ac (●) and dc (△) data for compound **5**. The solid line is drawn as a guide.

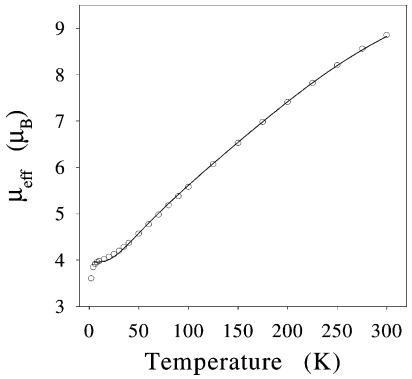

Figure 11. μ_{eff} vs T for compound **6**. The solid line is the fit of the data; see the text for the fit parameters.

For **6**, restrained in eicosane to prevent torquing, the μ_{eff} decreases gradually from 8.86 μ_B at 300 K to ∼3.97 μ_B at 10.0 K, where it almost plateaus, and then decreases to 3.61 μ_B at 5.00 K (Figure 11). The value of 8.86 μ_B at 300 K is significantly less than the spin-only ($g = 2$) value of 10.82 μ_B expected for a $Mn_3^{III}Mn_3^{IV}$ complex with noninteracting metal centers, indicating the presence of strong antiferromagnetic interactions within the molecule. The value at 10.0 K is very close to 3.87 μ_B, the spin-only value for $S = 3/2$, suggesting this might be the ground state, with the decrease below 10.0 K being due to zero-field splitting effects. Assuming idealized C_{3v} symmetry, four exchange parameters are required to describe the pairwise exchange interactions between the six metal centers. The resulting Heisenberg spin Hamiltonian is given by eq 9, where J_a ($Mn^{IV}Mn^{IV}$), J_b ($Mn^{III}Mn^{III}$), J_c, (adjacent $Mn^{III}Mn^{IV}$), and J_d (nonadjacent $Mn^{III}Mn^{IV}$) gauge the exchange interactions indicated, and are represented by blue, green, red, and yellow lines, respectively, in Figure 12.

$$\hat{H} = -2J_a(\hat{S}_1\cdot\hat{S}_2 + \hat{S}_2\cdot\hat{S}_3 + \hat{S}_1\cdot\hat{S}_3) - 2J_b(\hat{S}_4\cdot\hat{S}_5 + \hat{S}_5\cdot\hat{S}_6 + \hat{S}_4\cdot\hat{S}_6) - 2J_c(\hat{S}_1\cdot\hat{S}_4 + \hat{S}_1\cdot\hat{S}_6 + \hat{S}_2\cdot\hat{S}_5 + \hat{S}_2\cdot\hat{S}_6 + \hat{S}_3\cdot\hat{S}_4 + \hat{S}_3\cdot\hat{S}_5) - 2J_d(\hat{S}_2\cdot\hat{S}_4 + \hat{S}_3\cdot\hat{S}_6 + \hat{S}_1\cdot\hat{S}_5) \quad (9)$$

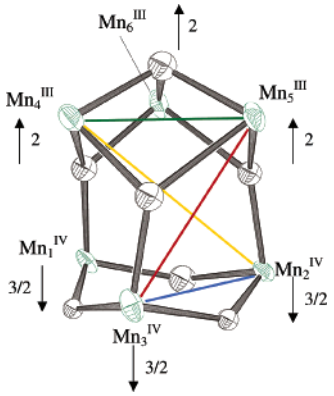

Figure 12. Exchange coupling scheme in complex **6**.

The geometric complexity of the molecule precludes the application of the Kambé equivalent operator method. However, the experimental data can be readily fit using a genetic algorithm fitting method described elsewhere,[30] which includes a full diagonalization of the spin Hamiltonian (981 states). The fit was performed using the data in the 15−300 K range, with a fixed TIP of 200 × 10^{-6} cm^3 mol^{-1} per Mn, and assuming J_d to be negligible since this interaction is mediated by four bonds instead of two as is the case for J_a, J_b, and J_c. The fit (the solid line in Figure 11) had parameter values of J_a = 22.9 cm^{-1}, J_b = 8.1 cm^{-1}, J_c = −18.7 cm^{-1}, and g = 2.0. These values were substituted into the spin Hamiltonian of the system, whose diagonalization provides the energies of all the spin states, and this confirmed the ground-state spin to be S = 3/2. The first and second excited states are S =5/2 and S = 7/2 states at 63.9 and 153.2 cm^{-1}, respectively, above the S = 3/2 ground state; the latter is thus well isolated. The spin alignments in this ground state are denoted by arrows in Figure 12: the three Mn^{III} ions of the cluster (top half of Figure 12) are ferromagnetically coupled to each other, and the three Mn^{IV} ions (bottom half of Figure 12) are also ferromagnetically coupled with each other, whereas interactions between the two types (i.e., $Mn^{III}\cdots Mn^{IV}$ interactions) are antiferromagnetic. This yields a spin of 6 for the top unit and 9/2 for the bottom one, and since they are aligned antiparallel, the net molecular spin is S = 3/2.

The values obtained for the exchange constants of compound **6** are consistent with the results reported for several compounds containing similar bridging motifs. The $[Mn^{III}_2(\mu_3\text{-}O)_2]^{2+}$ units in **6**, with interactions depicted in green in Figure 12, are comparable to similar units in the series of well-known distorted-cubane complexes of formula $[Mn_4O_3X(O_2CR)_3(dbm)_3]$ (X = F^-, Cl^-, Br^-, OH^-, etc.; R = Me, Et, Ph; dbm^- = the anion of dibenzoylmethane).[31] The exchange couplings between Mn^{III} ions in these compounds are always ferromagnetic with values ranging from 5 to 12 cm^{-1}, and the value of 8.1 cm^{-1} for this interaction in **6** falls within this range. Likewise, the $[Mn^{III}(\mu_3\text{-}O)Mn^{IV}]^{3+}$ units of complex **6** are analogous to similar units in these cubane complexes, where the interactions between the Mn^{III} and Mn^{IV} atoms are always antiferromagnetic, with values between −21 and −36 cm^{-1}, very close to the −18.7 cm^{-1} value obtained for J_c. Finally, the bridging mode found for the three Mn^{IV} ions, connected with one another through a single μ-oxide ion, is analogous to that found between the Mn^{IV} centers in adamantane-like compounds, for example, $[Mn_4O_6(L)_4]X_4$ (L = *N*,*N*-bis(2-pyridylmethyl)ethylamine or 1,4,7-triazacyclononane; X = ClO_4^-, Br^-, $CF_3SO_4^-$).[32] The exchange constant for that interaction was 14.5 cm^{-1}, of the same sign as and similar in magnitude to the J_a = 22.9 cm^{-1} in compound **6**.

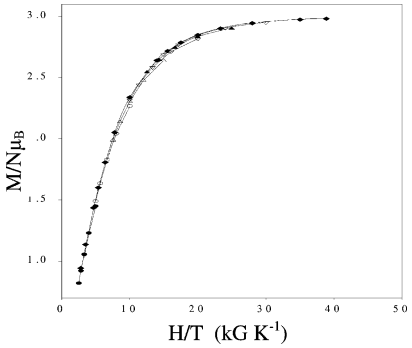

Figure 13. $M/N\mu_B$ vs H/T for complex **6**. The solid lines are the fit of the data; see the text for the fit parameters.

To confirm the S = 3/2 ground state deduced from the fit, and also to obtain the value of the ZFS parameter D, magnetization data were collected in the 1.80−25.0 K range with applied magnetic fields of 10−70 kG. The obtained data are plotted as reduced magnetization ($M/N\mu_B$) vs H/T in Figure 13. The expected saturation value for an S = 3/2 state with g = 2.00 is 3, and this is essentially what is observed. The data were fit by diagonalization of the spin Hamiltonian matrix assuming only the ground state to be populated at these temperatures, and incorporating ZFS and Zeeman interactions and employing a full powder average of the magnetization. The best fit (solid lines in Figure 13) was with S = 3/2, D = −0.792(7) cm^{-1}, and g = 2.00(1). The S = 3/2 ground state of **6** is thus confirmed.

EPR Spectroscopy of 6. X-band EPR spectra of **6** were recorded on a MeCN/toluene (1:2) glass in the 5.0−50 K range, and the resulting spectra are shown in Figure 14. The spectrum at 5.0 K displays the typical features of a slightly rhombic S = 3/2 system,[33] with $g_x > 4$, $g_y \approx 4$, and $g_z \approx 2$. Specifically, two primary signals can be seen at g = 1.9 and g = 3.7. The latter is too broad to allow clear resolution of

(30) O'Brien, T. A.; Cañada-Vilalta, C.; Christou, G.; Davidson, E. R. *J. Phys. Chem. A*, submitted for publication.

(31) (a) Wang, S.; Tsai, H.-L.; Folting, K.; Streib, W. E.; Hendrickson, D. N.; Christou, G. *Inorg. Chem.* **1996**, *35*, 7578. (b) Wemple, M. W.; Adams, D. M.; Hagen, K. S.; Folting, K.; Hendrickson, D. N.; Christou, G. *J. Chem. Soc., Chem. Commun.* **1995**, 1591. (c) Wemple, M. W.; Adams, D. M.; Folting, K.; Hendrickson, D. N.; Christou, G. *J. Am. Chem. Soc.* **1995**, *117*, 7275. (d) Wang, S.; Tsai, H.-L.; Hagen, K. S.; Hendrickson, D. N.; Christou, G. *J. Am. Chem. Soc.* **1994**, *116*, 8376. (e) Aromí, G.; Wemple, M. W.; Aubin, S. J.; Folting, K.; Hendrickson, D. N.; Christou, G. *J. Am. Chem. Soc.* **1998**, *120*, 5850. (f) Aubin, S. M. J.; Dilley, N. R.; Pardi, L.; Krzystek, J.; Wemple, M. W.; Brunel, L.-C.; Maple, M. B.; Christou, G.; Hendrickson, D. N. *J. Am. Chem. Soc.* **1998**, *120*, 4991.

(32) (a) Dube, C. E.; Wright, D. W.; Bonitatebus, P. J., Jr.; Pal, S.; Armstrong, W. H. *J. Am. Chem. Soc.* **1998**, *120*, 3704. (b) Hagen, K. S.; Westmoreland, T. D.; Scott, M. J.; Armstrong, W. H. *J. Am. Chem. Soc.* **1989**, *111*, 1907.

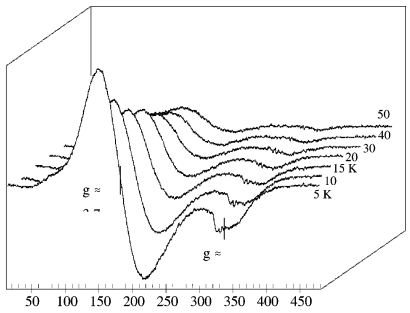

Figure 14. Variable-temperature X-band EPR spectra of compound **6** in a MeCN/toluene (1:2) glass.

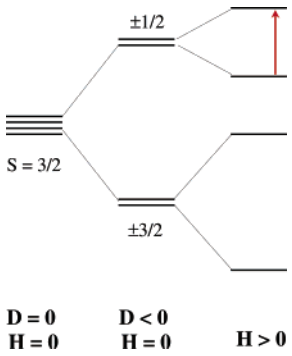

Figure 15. Splitting of the M_S levels of an $S = 3/2$ state when the axial ZFS parameter D is negative and when a field is applied. The arrow shows the transition detected in the EPR spectra.

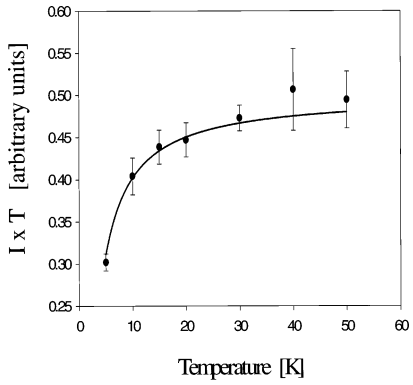

Figure 16. *IT* vs *T* plot for compound **6** using data obtained from the variable-temperature EPR spectra. The solid line is the fit of the data; see the text for the fit parameters.

another feature at lower fields. The EPR signal is due to the $M_s = \pm 1/2$ second Kramer doublet of the $S = 3/2$ system, which for a negative D is at higher energy than the $M_s = \pm 3/2$ doublet (Figure 15). Indeed, a plot of the variation of the intensity (I) of the EPR signal with temperature, shown as an *IT* vs *T* plot in Figure 16, confirms a negative sign of D. The increase in *IT* with *T* is caused by the increasing population of the $M_s = \pm 1/2$ doublet. The value of I was determined by double integration of the signal, corrected for the baseline.

By considering both the Curie behavior expected for an $M_s = \pm 1/2$ signal and the Boltzmann population of this doublet, which depends on the energy difference Δ between it and the first Kramer doublet ($M_s = \pm 3/2$), the following expression[34] can be derived:

$$IT \propto \frac{1}{1 + \exp(\Delta/kT)} \tag{10}$$

The energy gap (Δ) between the two Kramer doublets is given by eq 11, where D and E are the axial and rhombic zero-field splitting parameters, respectively.

$$\Delta = 2(D^2 + 2E^2)^{1/2} \tag{11}$$

Since compound **6** has virtual C_{3v} symmetry, the rhombic anisotropy should be small (i.e., $E \approx 0$), and the approximation $\Delta \approx |2D|$ was employed. Fitting of the experimental data to this expression (solid line in Figure 16) yields an estimate of $D = -1.4(3)$ cm^{-1}. This is in reasonable agreement with the value obtained by fitting the reduced magnetization data ($D = -0.79$ cm^{-1}), given the error bars on the EPR data from the uncertainty inherent in quantitating such broad signals. The main conclusions of the EPR study are that the D value is indeed negative, and its magnitude is in the region of -1 cm^{-1}. The -0.79 cm^{-1} value is considered more reliable to two decimal places.

Conclusions

The dicarboxylate ligand mpdp^{2-} has proven a flexible ligand and has allowed the synthesis of four new Mn compounds of different nuclearities and oxidation states. The carboxylate substitution reaction on preformed species is particularly convenient, as demonstrated in the preparation of $[Mn_2O(mpdp)(bpy)_2(H_2O)(MeCN)](ClO_4)_2$ (**3**) and $[Mn_3O(mpdp)_3(py)_3](ClO_4)$ (**4**). The dicarboxylate ligand can occupy the sites previously occupied by two monocarboxylate groups without noticeable strain being introduced, and thus the core is not transformed. The dicarboxylate can also be used in other types of reactions, such as the synthesis of $[Mn_3O(mpdp)_3(py)_3]$ (**5**) and the oxidation of either **3** or **4** with $NBu^n_4MnO_4$ that yielded the new, mixed-valent compound $[Mn_6O_7(mpdp)_3(bpy)_3](ClO_4)$ (**6**). The latter represents a new structural type in Mn chemistry. The magnetic properties of the Mn_2 and Mn_3 species are as expected for

(33) (a) Chandra, K.; Basu, P.; Ray, D.; Pal, S.; Chakravorty, A. *Inorg. Chem.* **1990**, *29*, 2423. (b) Ray, M.; Golombek, A. P.; Hendrich, M. P.; Yap, Gl. P. A.; Liable-Sands, L. M.; Rheingold, A. L.; Borovik, A. S. *Inorg. Chem.* **1999**, *38(13)*, 3110. (c) Kersting, B.; Siebert, D. *Inorg. Chem.* **1998**, *37*, 3820. (d) Munro, O. Q.; de Wet, M.; Pollak, H.; Van Wyk, J.; Marques, H. M. *J. Chem. Soc., Faraday Trans.* **1998**, *94(12)*, 1743. (e) Sorlie, M.; Christiansen, J.; Dean, D. R.; Hales, B. J. *J. Am. Chem. Soc.* **1999**, *121*, 9457. (f) Das, G.; Bharadwaj, P. K.; Ghosh, D.; Chaudhuri, B.; Banerjee, R. *Chem. Commun.* **2001**, *4*, 323.

(34) (a) Keutel, H.; Käpplinger, I.; Jäger, E.-G.; Grodzicki, M.; Schüneman, V.; Trautwein, A. X. *Inorg. Chem.* **1999**, *38*, 2320. (b) Hauser, C.; Glaser, T.; Bill, E.; Weyhermüller, T.; Wieghardt, K. *J. Am. Chem. Soc.* **2000**, *122*, 4352.

(35) (a) Wieghardt, K.; Bossek, U.; Ventur, D.; Weiss, J. *J. Chem. Soc., Chem. Commun.* **1985**, 347. (b) Wieghardt, K.; Bossek, U.; Nuber, B.; Weiss, J.; Bonvoisin, J.; Corbella, M.; Vitols, S. E.; Girerd, J. J. *J. Am. Chem. Soc.* **1988**, *110*, 7398.

(36) Sheats, J. E.; Czernuszewicz, R. S.; Dismukes, G. C.; Rheingold, A. L.; Petrouleas, V.; Stubbe, J.; Armstrong, W. H.; Beer, R. H. and Lippard, S. J. *J. Am. Chem. Soc.* **1987**, *109*, 1435.

(37) Wu, F. J.; Kurtz, D. M.; Hagen, K. S.; Nyman, P. D.; Debrunner, P. G.; Vankai, V. A. *Inorg. Chem.* **1990**, *29*, 5174.

(38) Gultneh, Y.; Ahvazi, B.; Khan, R.; Butcher, R. J.; Tuchagues, J. P. *Inorg. Chem.* **1995**, *34*, 3633.

these structural units. Compound **6**, however, has proven an interesting molecule from a magnetic point of view, providing rare examples of ferromagnetically coupled Mn^{III}_3 and Mn^{IV}_3 units, which then couple antiferromagnetically between them to give the overall $S = 3/2$ ground state. The analogue of compound **6** with monocarboxylates is not known, at least to date, and it is currently not evident whether its preparation and the stability of this Mn_6 species are dependent on the dicarboxylate nature of the $mpdp^{2-}$ ligand. In any event, it is clear that the use of dicarboxylates can be very beneficial in the synthesis of new Mn clusters, and their use in our work is continuing.

Acknowledgment. This work was supported by the National Science Foundation.

Supporting Information Available: X-ray crystallographic files in CIF format for complexes **3**·3MeCN, **4**, **5**·$2C_6H_6$, and **6**·3.5MeCN. This material is available free of charge via the Internet at http://pubs.acs.org.

IC034973M